Science Advances
AAAS

advances.sciencemag.org/cgi/content/full/5/9/eaax0365/DC1

Supplementary Materials for

Large-scale RNAi screen identified Dhpr as a regulator of mitochondrial morphology and tissue homeostasis

Jia Zhou, Lingna Xu, Xiuying Duan, Wei Liu, Xiaocui Zhao, Xi Wang, Weina Shang, Xuefei Fang, Huan Yang, Lijun Jia, Jian Bai, Jiayao Zhao, Liquan Wang, Chao Tong*

*Corresponding author. Email: ctong@zju.edu.cn

Published 18 September 2019, *Sci. Adv.* **5**, eaax0365 (2019)
DOI: 10.1126/sciadv.aax0365

The PDF file includes:

Supplementary Materials and Methods
Fig. S1. The complex analysis of the hits from the mitochondrial morphology screening.
Fig. S2. The mitochondrial morphology in the fat body tissues with indicated gene RNAi is shown.
Fig. S3. Sixteen genes encoding proteasome components were identified in this mitochondrial morphology screening.
Fig. S4. Twenty-seven genes encoding spliceosome components were identified in this mitochondrial morphology screening.
Fig. S5. The reduction of the enzymes involved in tyrosine and lysine metabolism led to abnormal mitochondrial morphology.
Fig. S6. Loss of *Dhpr* leads to the reduction of life span and increase of the ROS production.
Fig. S7. The overexpression of *Pink1* or *park* partially rescues muscle defects caused by *Dhpr* RNAi.
Fig. S8. The genetic interaction between *Dhpr* and genes whose products consume or produce BH4.
Fig. S9. The genetic interaction between *Dhpr* and other core machinery of mitochondrial fusion and fission.
Fig. S10. The model of how Dhpr regulates mitochondrial morphology.

Other Supplementary Material for this manuscript includes the following:

(available at advances.sciencemag.org/cgi/content/full/5/9/eaax0365/DC1)

Table S1 (Microsoft Excel format). The list of the RNAi lines used in this screening and their corresponding genes.
Table S2 (Microsoft Excel format). The annotation of the phenotypes and the quantification data.

Table S3 (Microsoft Excel format). The list of genes that had two or three independent RNAi lines and genes that had been reported to be involved in regulating mitochondria.
Table S4 (Microsoft Excel format). The list of protein complexes required for mitochondrial morphology maintenance.
Table S5 (Microsoft Excel format). The lists of genes encoding spliceosome, proteasome, and electron transfer chain components that have been identified in this screen.

Supplemental Materials and Method

Lifespan analysis.

Flies of each genotype were collected and housed at a density of 20 male per vial. All flies were cultured in a humidified, temperature-controlled incubator (60-70% and 25℃, respectively) with 12 h on/off light cycle. The flies were transferred to fresh food and scored every 2-3 days.

Immunostaining and image analysis.

Fly tissues were dissected and fixed for half an hour with 4% paraformaldehyde in PBS. For the samples examined without antibody immunostaining, samples were rinsed three times with PBST (0.3% Triton X-100 in PBS) and then mounted in 80% glycerol with DAPI. Mitochondria were detected by mitoGFP signals. To carry out antibody immunostaining, samples were rinsed three times with PBST and blocked with 5% BSA in PBST for 30 min at room temperature. Primary antibody was diluted in PBST with 5% BSA and incubated overnight at 4℃. Primary antibodies used were: rabbit anti-HA (Cell Signaling, 3724S) diluted 1:1000, mouse anti-V5 (Invitrogen, R96025) diluted 1:500 and mouse anti- α -TH (ImmunoStar, 22941) diluted 1:400. Samples were then rinsed three times with PBST and incubated with secondary antibodies and/or stains for 1h at room temperature. All secondary antibodies were diluted 1:500 in PBST with 5% BSA. Secondary antibodies used were: anti-rabbit or anti-mouse AlexaFlour-488 (Invitrogen, A-21206 and A-21202); anti-rabbit or anti-mouse AlexaFlour-594 (Invitrogen, A-21207 and A-21203); anti-rabbit or anti-mouse AlexaFlour-647 (Invitrogen, A-31573 and A-21235). Samples were then rinsed three times and mounted in 80% glycerol with DAPI. All the samples were imaged on a LSM710 confocal microscope (Carl Zeiss, LSM710, Oberkochen, Germany) with a Plan-Apochromat X63 oil immersion (Carl Zeiss, 1262466A).

Light and electron microscopy.

To examine the morphology of the flight muscles, the fly thoraxes were dissected and fixed in 2.5% glutaraldehyde (Electron Microscopy Sciences, 16020) and 2.0% paraformaldehyde (Electron Microscopy Sciences, 15710) in 0.1 M cacodylate buffer (Electron Microscopy Sciences, 12201) for 72 to 96 hours at 4℃. Samples were rinsed three times with 0.1 M PBS and then post-fixed in 1% osmium tetroxide (Electron Microscopy Sciences, 19152) for 2 hours in 0.1 M PBS. After rinsing three times with 0.1 M PBS, samples were dehydrated through a graded ethanol series (50%, 70%, 80%, 90%, 95% and 100%, respectively). Samples were then dehydrated in propylene oxide (PO) (Sigma, 82320) for 30 min. After infiltration with a graded series of Eponate 12 resin (50% and 75% in PO), samples were embedded in fresh and pure Eponate 12 resin made up from Embed 812 (Electron Microscopy Sciences, 14900), DDSA (Electron Microscopy Sciences, 13710), NMA (Electron Microscopy Sciences, 19000) and DMP-30 (Electron Microscopy Sciences, 13600) and polymerized at 65℃ for 48 hours. Semi-thin sections (1.5 um) were cut on Leica EM UC7 ultramicrotome (Leica Microsystems, Vienna, Austria) and stained with toluidine blue (Electron Microscopy Sciences, 22050) and examine under light microscopy. The 50-nm thin sections were stained with 4% uranyl acetate (Electron Microscopy Sciences, 22400) and 2.5% lead nitrate (Electron Microscopy Sciences, 17800) for electron microscopy analysis (Hitachi Ltd., HT7700, Tokyo, Japan).

ROS staining.

Fat-body tissues were dissected from third instar larvae in cold Drosophila Schneider's Medium (DSM) (Thermo Fisher Scientific, S0146). For DCFH-DA (Beyotime Biotechnology, S0033) staining, samples were incubated with DCFH-DA (10uM in DSM) for 15 min at room temperature in a dark chamber on shaker (speed 120 round per min). After rinsing three times for 2 min each time (hoechst33258 added to DSM at the last time), samples were quickly mounted in DSM and imaged within 10-15 min. Quantification of staining is done using Image J.

JC-1 staining.

Flight muscle tissues were dissected in cold Drosophila Schneider's Medium (DSM) (Thermo Fisher Scientific, S0146). Samples were incubated with JC-1 (5ug/ml) (Beyotime Biotechnology, C2006) for 20 min at 37℃ in a dark chamber. In the CCCP treatment group, samples should be firstly incubated in DSM with 10um CCCP and then incubated with JC-1. After rinsing twice for about 10 sec each time, samples were quickly mounted in DSM and imaged within 10-15 min. The JC-1 aggregate form (red) has absorption/emission maxima of 585/590 nm, while the JC-1 monomeric form (green) has 514/529 nm.

ATP assays.

ATP levels were measured by using the ATP assay kit (Beyotime Biotechnology, S0026). The standard manufacturer's protocols were followed. Briefly, fat-body tissues dissected from 10 third *in star* larvae for each genotype were lysed in ATP lysis buffer. After centrifugation, the supernatants of each sample were harvested and the ATP levels were measured by using the Synergy Neo2 plate reader (Bio Tek Inc. Winooski, Vermont, USA). The values were normalized to protein content measured by the Pierce BCA protein assay kit (Thermo Fisher, 23227). The measurements were repeated at least three times for each genotype.

Climbing assay.

Age matched male flies (10 per vial) were transferred into 20-cm-long vials and incubated at room temperature for 1 h. Then the flies were completely tapped down to the bottom of the vials. The climbing time was recorded when more than half of flies had passed the 10-cm finish line. Ten different groups of flies were repeated and each group were performed for five trials. The average climbing time for each genotype was calculated. The climbing assay was performed when the flies were 3 days old, 10 days old, 20 days old, or 30 days old.

Quantitative real-time PCR.

Total RNA was extracted with TRIzol reagent (Invitrogen, 15596018) by following standard manufacturer's protocols. The cDNA synthesis was carried out by using the M-MLV Reverse Transcriptase (Thermo Fisher, 28025-013). Power SYBR Green master mix (Applied Biosystems, Life technologies, 4367659) were used in an Applied Biosystems 7500 Real-Time PCR System (Applied Biosystems Inc, Carlsbad, California). The primers used for each target were: *Dhpr*: F: 5'-CAATTATTGGGTTGGCAGCA-3', R: 5'-CCACATGAGATCGGCATTCT-3'; *RpLP0*: F: 5'-CTAAGCTGTCGCACAAATGGC-3', R: 5'-ATCTCCTTGCGCTTCTTGGA-3', *Nos*: F: 5'-GCCAGAGCATTGAGACCACTGG-3', R: 5'-ATGCTTGGCATCTGTGCGTT-3'.

Western blotting assay.

The standard procedures of western blotting were followed. Fat body tissue/ thorax tissue of each genotype flies were homogenized in lysis buffer and protein concentration was measured using the Pierce BCA protein assay kit (Thermo Fisher, 23227). Proteins were separated by SDS-PAGE and transferred onto a PVDF membrane. The membrane was blocked with 5% non-fat milk in TBST buffer (0.1% Tween 20 in TBS) and incubated with primary antibodies in 5% non-fat milk in TBST buffer overnight at 4℃. The primary antibodies used were as follows: anti-Drp1 (Cell Signaling, 8570S) diluted 1:1000, anti-Mitofusin 2 (Aviva Systems Biology, ABIN2775407) diluted 1:1000 and anti-α-tubulin (Beyotime Biotechnology, AT819) diluted 1:500. Although they were generated with antigens from the mammalian orthologs, the antibodies could successfully detect fly proteins. The membrane was then washed three times with TBST buffer and incubated with secondary antibodies and/or stains for 1h at room temperature. The secondary antibodies used were anti-rabbit/mouse-HRP (Jackson ImmunoResearch Laboratories, 111-035-003 and 115-035-003) diluted 1:5000. The membrane was washed three times with TBST

buffer and then incubated with ECL reagent and exposed. Quantification of protein bands was done using the Image J software.

Fly genotypes.

The genotypes of the fly strains generated in the paper are as followed:

Fig. 1 C, ***Attp2****: CgGal4 UAS-mitoGFP / +; UAS-attp2 / +.* **D,** ***ND-51:*** *CgGal4 UAS-mitoGFP / +; UAS-ND-51 RNAi / +.* **E,** ***Tom40:*** *CgGal4 UAS-mitoGFP / +; UAS-Tom40 RNAi / +.* **F,** ***Rpn11:*** *CgGal4 UAS-mitoGFP / +; UAS-Rpn11 RNAi / +.* **G,** ***CG13442:*** *CgGal4 UAS-mitoGFP / +; UAS-CG3270 RNAi / +.* **H,** ***LKRSDH:*** *CgGal4 UAS-mitoGFP / UAS-LKRSDH RNAi.* **I,** ***Ncoa6:*** *CgGal4 UAS-mitoGFP / +; UAS-Ncoa6 RNAi / +.* **J,** ***CG12951:*** *CgGal4 UAS-mitoGFP / UAS-CG12951 RNAi.* **K,** ***xit:*** *CgGal4 UAS-mitoGFP / +; UAS-xit RNAi / +.* **L,** ***Drp1 :****CgGal4 UAS-mitoGFP / UAS-Drp1 RNAi.* **M,** ***Marf:*** *CgGal4 UAS-mitoGFP / +; UAS-marf RNAi / +.* **N,** ***Opa1:*** *CgGal4 UAS-mitoGFP / +; UAS-Opa1 RNAi / +.* **O,** ***zuc:*** *CgGal4 UAS-mitoGFP / UAS-zuc RNAi.* **P,** ***Warts:*** *CgGal4 UAS-mitoGFP / +; UAS-Warts RNAi / +.* **Q,** ***YME1L:*** *CgGal4 UAS-mitoGFP / +; UAS-YME1L RNAi / +.* **R,** ***Chchd3:*** *CgGal4 UAS-mitoGFP / +; UAS-Chchd3 RNAi / +.* **S,** ***MSP300:*** *CgGal4 UAS-mitoGFP / +; UAS-MSP300 RNAi / +.* **T,** ***milt:*** *CgGal4 UAS-mitoGFP / +; UAS-milt RNAi / +.* **U,** ***Pink1:*** *CgGal4 UAS-mitoGFP / +; UAS-Pink1 RNAi / +.* **V,** ***park:*** *CgGal4 UAS-mitoGFP / +; UAS-park RNAi / +.*

Fig. 2 A, ***CTRL:*** *CgGal4 UAS-mitoGFP / +; UAS-attp2 / +.* **B,** ***ND-42:*** *CgGal4 UAS-mitoGFP / +; UAS-ND42 RNAi / +.* **C,** ***ND-15:*** *CgGal4 UAS-mitoGFP / UAS-ND-15 RNAi.* **D,** ***ND-51:*** *CgGal4 UAS-mitoGFP / +; UAS-ND-51 RNAi / +.* **E,** ***ND-23:*** *CgGal4 UAS-mitoGFP / UAS-ND-23 RNAi.* **F,** ***Sdhc:*** *CgGal4 UAS-mitoGFP / UAS-Sdhc RNAi.* **G,** ***UQCR-Q:*** *CgGal4 UAS-mitoGFP / +; UAS-UQCR-Q RNAi / +.* **H,** ***Cchl:*** *CgGal4 UAS-mitoGFP / +; UAS-Cchl RNAi / +.* **I,** ***cype:*** *CgGal4 UAS-mitoGFP / +; UAS-cype RNAi / +.* **J,** ***ATPsynB:*** *CgGal4 UAS-mitoGFP / +; UAS-ATPsynB RNAi / +.* **K and L,** ***CTP syn:*** *CgGal4 UAS-mitoGFP / +; UAS-CTP syn RNAi / +.* **M and U,** ***CTRL:*** *CgGal4 / +; UAS-attp2 / +.* **N,** ***ND-49 RNAi:***

CgGal4 / +; UAS-ND-49 RNAi / +. **O, *NP15.6 RNAi:*** *CgGal4 / +; UAS-NP 15.6 RNAi / +*. **P, *Cchl RNAi:*** *CgGal4 / +; UAS-Cchl RNAi / +*. **Q and V, *CTP syn RNAi:*** *CgGal4 / +; UAS-CTP syn RNAi / +*. **W, *ND-15 RNAi:*** *CgGal4 / UAS-ND-15 RNAi.*

Fig. 3 A and G, *CTRL:* *CgGal4 UAS-mitoGFP / +; UAS-attp2 / +*. **B, *Pink1 RNAi:*** *CgGal4 UAS-mitoGFP / +; UAS-Pink1 RNAi / +*. **C, *park RNAi:*** *CgGal4 UAS-mitoGFP / +; UAS-park RNAi / +*. **D, *ben RNAi:*** *CgGal4 UAS-mitoGFP / +; UAS-ben RNAi / +*. **E and H, *Dhpr RNAi:*** *CgGal4 UAS-mitoGFP / UAS-Dhpr RNAi.* **F, *Dhpr RNAi; Dhpr OE:*** *CgGal4 UAS-mitoGFP / UAS-Dhpr RNAi; UAS-Dhpr 3HA / +*. **K, K' and Q, W^{1118}:** W^{1118}. **L, L' and R, $Dhpr^{17-4}$:** W^{1118}; $Dhpr^{17-4}$. **M, M' and S, $Pink1^{[B9]}$:** *W* Pink1*$^{[B9]}$ */ Y.* **N and N', *Dhpr G; Dhpr*$^{17-4}$:** *pattB-Dhpr G / +;* $Dhpr^{17-4}$. **U, *CTRL:*** *UAS-attp40 / +; PleGal4 UAS-mitoGFP / UAS-Dcr-2.* **V, *Dhpr RNAi; Dcr-2 OE:*** *UAS-Dhpr RNAi / +; PleGal4 UAS-mitoGFP / UAS-Dcr-2.* **W, $Pink1^{[B9]}$:** *Pink1*$^{[B9]}$ */ Y; PleGal4 UAS-mitoGFP / +*.

Fig. 4 A, *CTRL:* *CgGal4 UAS-mitoGFP / +; UAS-attp2 / +*. **B, *Dhpr RNAi:*** *CgGal4 UAS-mitoGFP / UAS-Dhpr RNAi.* **C, *Pink1 OE:*** *CgGal4 UAS-mitoGFP / +; UAS-Pink1 / +*. **D, *park-V5 OE:*** *CgGal4 UAS-mitoGFP / +; UAS-park-V5 / +*. **E, *Dhpr RNAi; Pink1 OE:*** *CgGal4 UAS-mitoGFP / UAS-Dhpr RNAi; UAS-Pink1 / +*. **F, *Dhpr RNAi; park-V5 OE:*** *CgGal4 UAS-mitoGFP / UAS-Dhpr RNAi; UAS-park-V5 / +*. **G, *Dhpr OE:*** *CgGal4 UAS-mitoGFP / +; UAS-Dhpr-3HA / +*. **H, *Pink1 RNAi; Dhpr OE:*** *CgGal4 UAS-mitoGFP / +; UAS-Pink1 RNAi / UAS-Dhpr-3HA.* **J and J', *CTRL:*** *UAS-attp40 / +; Mef2Gal4 / +*. **K and K', *Dhpr RNAi:*** *UAS-Dhpr RNAi / +; Mef2Gal4 / +*. **L and L', *Pink1 OE:*** *Mef2Gal4 / UAS-Pink1.* **M and M', *Dhpr RNAi; Pink1 OE:*** *UAS-Dhpr RNAi / +; Mef2Gal4/ UAS-Pink1.* **N and N', *park-V5 OE:*** *Mef2Gal4 / UAS-park-V5.* **O, O' and O'', *Dhpr RNAi; park-V5 OE:*** *UAS-Dhpr RNAi / +; Mef2Gal4 / UAS-park-V5.* **R, R' and R'', $Pink1^{[B9]}$:** W^{*} *Pink1*$^{[B9]}$ */ Y.* **S and S', *Pink1*$^{[B9]}$*; Dhpr RNAi:*** *Pink1*$^{[B9]}$ */ Y; UAS-Dhpr RNAi / +; Mef2Gal4 / +*.

Fig. 5 A, ***CTRL:*** *CgGal4 UAS-mitoGFP / +; UAS-attp2 / +.* **B,** ***Dhpr RNAi:*** *CgGal4 UAS-mitoGFP / UAS-Dhpr RNAi.* **C,** ***Dhpr OE:*** *CgGal4 UAS-mitoGFP / +; UAS-Dhpr-3HA / +.* **D,** ***Dhpr^{G16D}-3HA OE:*** *CgGal4 UAS-mitoGFP / +; UAS-Dhpr^{G16D}-3HA / +.* **E and E',** ***CTRL:*** *Mef2Gal4 / UAS-attp2.* **F and F',** ***Dhpr RNAi:*** *UAS-Dhpr RNAi / +; Mef2Gal4 / +.* **G and G',** ***Dhpr OE:*** *Mef2Gal4 / UAS-Dhpr-3HA.* **H and H',** ***Dhpr^{G16D}-3HA OE:*** *Mef2Gal4 / UAS-Dhpr^{G16D}-3HA.* **I,** ***Dhpr RNAi; Dhpr OE:*** *CgGal4 UAS-mitoGFP / UAS-Dhpr RNAi; UAS-Dhpr-3HA / +.* **J,** ***Dhpr RNAi; Dhpr^{G16D}-3HA OE:*** *CgGal4 UAS-mitoGFP / UAS-Dhpr RNAi; UAS-Dhpr^{G16D}-3HA / +.* **K,** ***Nos RNAi:*** *CgGal4 UAS-mitoGFP / +; UAS-Nos RNAi / +.* **L,** ***Dhpr RNAi; Nos RNAi:*** *CgGal4 UAS-mitoGFP / UAS-Dhpr RNAi; UAS-Nos RNAi / +.* **M and M',** ***Dhpr RNAi; Dhpr OE:*** *UAS-Dhpr RNAi / +; Mef2Gal4 / UAS-Dhpr-3HA.* **N and N',** ***Dhpr RNAi; Dhpr^{G16D}-3HA OE:*** *UAS-Dhpr RNAi / +; Mef2Gal4 / UAS-Dhpr^{G16D}-3HA.* **O and O',** ***Nos RNAi:*** *Mef2Gal4 / UAS-Nos RNAi.* **P and P',** ***Dhpr RNAi; Nos RNAi:*** *UAS-Dhpr RNAi / +; Mef2Gal4 / UAS-Nos RNAi.*

Fig. 6 A, ***CTRL:*** *CgGal4 UAS-mitoGFP / +; UAS-attp2 / +.* **B,** ***Dhpr RNAi:*** *CgGal4 UAS-mitoGFP / UAS-Dhpr RNAi.* **C,** ***Drp1 OE:*** *CgGal4 UAS-mitoGFP / +; UAS-Drp1 / +.* **D,** ***Dhpr RNAi; Drp1 OE:*** *CgGal4 UAS-mitoGFP / UAS-Dhpr RNAi; UAS-Drp1 / +.* **E and E',** ***CTRL:*** *Mef2Gal4 / UAS-attp2.* **F and F',** ***Dhpr RNAi:*** *UAS-Dhpr RNAi / +; Mef2Gal4 / +.* **G and G',** ***Drp1 OE:*** *Mef2Gal4 / UAS-Drp1.* **H and H',** ***Dhpr RNAi; Drp1 OE:*** *UAS-Dhpr RNAi / +; Mef2Gal4 / UAS-Drp1.* **N,** ***Drp1 RNAi:*** *CgGal4 UAS-mitoGFP / +; UAS-Drp1 RNAi / +.* **O,** ***Drp1 RNAi; Drp1 OE:*** *CgGal4 UAS-mitoGFP / +; UAS-Drp1 RNAi / UAS-Drp1.* **P,** ***Drp1^{C643A}-3HA OE:*** *CgGal4 UAS-mitoGFP / +; UAS-Drp1^{C643A}-3HA / +.* **Q,** ***Drp1 RNAi; Drp1^{C643A}-3HA OE:*** *CgGal4 UAS-mitoGFP / +; UAS-Drp1 RNAi / UAS-Drp1^{C643A}-3HA.* **S,** ***Dhpr RNAi; Drp1^{C643A}-3HA OE:*** *CgGal4 UAS-mitoGFP / UAS-Dhpr RNAi; UAS-Drp1^{C643A}-3HA / +.*

Fig. S2 A-D, ***Attp2 :****CgGal4 UAS-mitoGFP / +; attp2 / +.* **E,** ***CG33650:*** *CgGal4*

UAS-mitoGFP / +; UAS-CG33650 RNAi / +. **F, *CG6050:*** *CgGal4 UAS-mitoGFP / +; UAS-CG6050 RNAi / +*. **G, *CG6512:*** *CgGal4 UAS-mitoGFP / +; UAS-CG6512 RNAi / +*. **H, *CG10920:*** *CgGal4 UAS-mitoGFP / +; UAS-CG10920 RNAi / +*. **I, *CG3057:*** *CgGal4 UAS-mitoGFP / UAS-CG3057 RNAi.* **J, *CG6851:*** *CgGal4 UAS-mitoGFP / +; UAS-CG6851 RNAi / +*. **K, *porin:*** *CgGal4 UAS-mitoGFP / +; UAS-porin RNAi / +*. **L, *CG7834:*** *CgGal4 UAS-mitoGFP / +; UAS-CG7834 RNAi / +*. **M, *CG12140:*** *CgGal4 UAS-mitoGFP / UAS-CG12140 RNAi.* **N, *CG3140:*** *CgGal4 UAS-mitoGFP / UAS-CG3140 RNAi.* **O, *CG3835:*** *CgGal4 UAS-mitoGFP / UAS-CG3835 RNAi.* **P, *CG2718:*** *CgGal4 UAS-mitoGFP / UAS-CG2718 RNAi.* **Q, *CG11876:*** *CgGal4 UAS-mitoGFP / UAS-CG11876 RNAi.* **R, *CG6459:*** *CgGal4 UAS-mitoGFP / +; UAS-CG6459 RNAi / +*. **S, *Pex1:*** *CgGal4 UAS-mitoGFP / +; UAS-Pex1 RNAi / +*. **T, *Pex13:*** *CgGal4 UAS-mitoGFP / +; UAS-Pex13 RNAi / +*. **U, *Pex19:*** *CgGal4 UAS-mitoGFP / +; UAS-Pex19 RNAi / +*. **V, *CRAT:*** *CgGal4 UAS-mitoGFP / UAS-CRAT RNAi.* **W, *Mfe2:*** *CgGal4 UAS-mitoGFP / UAS-Mfe2 RNAi.* **X, *Hmgcr:*** *CgGal4 UAS-mitoGFP / UAS-Hmgcr RNAi.*

Fig. S3 B, *Rpn1:* *CgGal4 UAS-mitoGFP / +; UAS-Rpn1 RNAi / +*. **C, *Rpn3:*** *CgGal4 UAS-mitoGFP / +; UAS-Rpn3 RNAi / +*. **D, *Rpn6:*** *CgGal4 UAS-mitoGFP / +; UAS-Rpn6 RNAi / +*. **E, *Rpn7:*** *CgGal4 UAS-mitoGFP / +; UAS-Rpn7 RNAi / +*. **F, *Rpn8:*** *CgGal4 UAS-mitoGFP / +; UAS-Rpn8 RNAi / +*. **G, *Rpn9:*** *CgGal4 UAS-mitoGFP / +; UAS-Rpn9 / +*. **H, *Rpn11:*** *CgGal4 UAS-mitoGFP / +; UAS-Rpn11 RNAi / +*. **I, *Rpn12:*** *CgGal4 UAS-mitoGFP / +; UAS-Rpn12 RNAi / +*. **J, *Rpt2:*** *CgGal4 UAS-mitoGFP / +; UAS-Rpt2 RNAi / +*. **K, *Rpt3:*** *CgGal4 UAS-mitoGFP / +; UAS-Rpt3 RNAi / +*. **L, *Rpt6:*** *CgGal4 UAS-mitoGFP / +; UAS-Rpt6 RNAi / +*. **M, *Prosα5:*** *CgGal4 UAS-mitoGFP / +; UAS-Prosα5 RNAi / +.* **N, *Prosα7:*** *CgGal4 UAS-mitoGFP / +; UAS-Prosα7 RNAi / +*. **O, *Prosβ1:*** *CgGal4 UAS-mitoGFP / +; UAS-Prosβ1 RNAi / +.* **P, *Prosβ5:*** *CgGal4 UAS-mitoGFP / +; UAS-Prosβ5 RNAi / +.* **Q, *Prosβ6:*** *CgGal4 UAS-mitoGFP / +; UAS-Prosβ6 RNAi / +.* **R, R' and R'', *CTRL:*** *CgGal4 / +; UAS-attp2 / +*. **S, S' and S'', *Prosα7:*** *CgGal4 / +;*

UAS-Prosα7 RNAi / +. **T, T' and T'', *Rpn11:*** *CgGal4 / +; UAS-Rpn11 RNAi / +.*

Fig. S4 B, *SmB:* *CgGal4 UAS-mitoGFP / UAS-SmB RNAi.* **C, *SmD3:*** *CgGal4 UAS-mitoGFP / +; UAS-SmD3 RNAi / +.* **D, *snRNP-U1-70K:*** *CgGal4 UAS-mitoGFP / +; UAS-snRNP-U1-70K RNAi / +.* **E, *snRNP-U1-C:*** *CgGal4 UAS-mitoGFP / +; UAS-snRNP-U1-C / +.* **F, *U2A:*** *CgGal4 UAS-mitoGFP / +; UAS-U2A RNAi / +.* **G, *U2af38:*** *CgGal4 UAS-mitoGFP / +; UAS-U2af38 RNAi / +.* **H, *Sf3a1:*** *CgGal4 UAS-mitoGFP / +; UAS-Sf3a1 RNAi / +.* **I, *Sf3b2:*** *CgGal4 UAS-mitoGFP / +; UAS-Sf3b2 RNAi / +.* **J, *Sf3b5:*** *CgGal4 UAS-mitoGFP / +; UAS-Sf3b5 RNAi / +.* **K, *noi:*** *CgGal4 UAS-mitoGFP / +; UAS-noi RNAi / +.* **L, *LSm7:*** *CgGal4 UAS-mitoGFP / UAS-LSm7 RNAi.* **M, *CG2021:*** *CgGal4 UAS-mitoGFP / UAS-CG2021 RNAi.* **N, *Prp3:*** *CgGal4 UAS-mitoGFP / UAS-Prp3 RNAi.* **O, *l(3)72Ab:*** *CgGal4 UAS-mitoGFP / +; UAS-l(3)72Ab RNAi / +.* **P, *CG6841:*** *CgGal4 UAS-mitoGFP / UAS-CG6841 RNAi.* **Q, *Prp8:*** *CgGal4 UAS-mitoGFP / +; UAS-Prp8 RNAi / +.* **R, *CG6015:*** *CgGal4 UAS-mitoGFP / +; UAS-CG6015 RNAi / +.* **S, *Bx42:*** *CgGal4 UAS-mitoGFP / +; UAS-Bx42 RNAi / +.* **T, *crn:*** *CgGal4 UAS-mitoGFP / +; UAS-crn RNAi / +.* **U, *CG9667:*** *CgGal4 UAS-mitoGFP / +; UAS-CG9667 RNAi / +.* **V, *Hrb98DE:*** *CgGal4 UAS-mitoGFP / +; UAS-Hrb98DE RNAi / +.* **W, *Ref1:*** *CgGal4 UAS-mitoGFP / +; UAS-Ref1 RNAi / +.* **X, *Prp19:*** *CgGal4 UAS-mitoGFP / +; UAS-Prp19 RNAi / +.* **Y, *Hsc70-1:*** *CgGal4 UAS-mitoGFP / +; UAS-Hsc70-1 RNAi / +.* **Z, *Hsc70-2:*** *CgGal4 UAS-mitoGFP / +; UAS-HSC70-2 RNAi / +.* **Z', *Hsc70-4:*** *CgGal4 UAS-mitoGFP / +; UAS-Hsc70-4 RNAi / +.* **Z'', *CG2685:*** *CgGal4 UAS-mitoGFP / +; UAS-CG2685 RNAi / +.*

Fig. S5 B, I and M, *CTRL:* *CgGal4 UAS-mitoGFP / +; UAS-attp2 / +.* **C, *Got1:*** *CgGal4 UAS-mitoGFP / +; UAS-Got1 / +.* **D, *hgo:*** *CgGal4 UAS-mitoGFP / UAS-hgo RNAi.* **E, *GstZ2:*** *CgGal4 UAS-mitoGFP / UAS-GstZ2.* **F, *Faa:*** *CgGal4 UAS-mitoGFP / UAS-Faa RNAi.* **G, *ple:*** *CgGal4 UAS-mitoGFP / +; UAS-ple RNAi / +.* **J, *LKRSDH:*** *CgGal4 UAS-mitoGFP / UAS-LKRSDH RNAi.* **K, *CG9629:*** *CgGal4*

UAS-mitoGFP / UAS-CG9629 RNAi. **N, *G9a:*** *CgGal4 UAS-mitoGFP / +; UAS-G9a RNAi / +.* **O, *eIF2γ:*** *CgGal4 UAS-mitoGFP / +; UAS-eIF2γ RNAi / +.* **P, *ash1:*** *CgGal4 UAS-mitoGFP / +; UAS-ash1 RNAi / +.* **Q, *CG10814:*** *CgGal4 UAS-mitoGFP / +; UAS-CG10814 / +.*

Fig. S6 A: *CgGal4 UAS-ManII-GFP / +; UAS-attp2 / +.* **B:** *CgGal4 UAS-GFP-SKL / +; UAS-attp2 / +.* **C:** *CgGal4 / +; UAS-RFP-KDEL / UAS-attp2.* **D:** *CgGal4 UAS-ManII-GFP / UAS-Dhpr RNAi.* **E:** *CgGal4 UAS-GFP-SKL / UAS-Dhpr RNAi.* **F:** *CgGal4 / UAS-Dhpr RNAi; UAS-RFP-KDEL / +.* **L** and **X, *W^{1118}:*** *W^{1118} / +; UAS-gstD1-GFP / +.* **M** and **Y, *$Dhpr^{17-4}$:*** *UAS-gstD1-GFP / +; $Dhpr^{17-4}$.* **N, *$Pink1^{[B9]}$:*** *$Pink1^{[B9]}$ / Y; UAS-gstD1-GFP / +.* **P, *CTRL:*** *CgGal4 / +; UAS-attp2 / +.* **Q, *Dhpr RNAi:*** *CgGal4 / UAS-Dhpr RNAi.* **T** and **V,** *W^{1118}.* **U,** *W^{1118}; $Dhpr^{17-4}$.*

Fig. S7 B and B', *CTRL:* *Mef2Gal4 / UAS-attp2.* **C, C' and C', *Dhpr RNAi:*** *UAS-Dhpr RNAi / +; Mef2Gal4 / +.* **D and D', *Pink1 OE:*** *Mef2Gal4 / UAS-Pink1.* **E and E', *park-V5 OE:*** *Mef2Gal4 / UAS-park-V5.* **F, F' and F'', *Dhpr RNAi; Pink OE:*** *Dhpr RNAi / +; Mef2Gal4 / UAS-Pink OE.* **G, G' and G'', *Dhpr RNAi; park-V5 OE:*** *Dhpr RNAi / +; Mef2Gal4 / UAS-park-V5.* **M, M' and M'':** *CgGal4 UAS-mitoGFP / pattB-Dhpr G / +.*

Fig. S8 C, *CTRL:* *CgGal4 UAS-mitoGFP / +; UAS-attp2 / +.* **D, *Dhpr RNAi:*** *CgGal4 UAS-mitoGFP / UAS-Dhpr RNAi.* **E, *Pu RNAi:*** *CgGal4 UAS-mitoGFP / +; UAS-Pu RNAi / +.* **F, *Dhpr RNAi; Pu RNAi:*** *CgGal4 UAS-mitoGFP / UAS-Dhpr RNAi; UAS-Pu RNAi / +.* **G, *hn RNAi:*** *CgGal4 UAS-mitoGFP / +; UAS-hn RNAi / +.* **H, *Trh RNAi:*** *CgGal4 UAS-mitoGFP / +; UAS-Trh RNAi / +.* **I, *ple RNAi:*** *CgGal4 UAS-mitoGFP / +; UAS-ple RNAi / +.* **J, *Dhpr RNAi; hn RNAi:*** *CgGal4 UAS-mitoGFP / UAS-Dhpr RNAi; UAS-hn RNAi / +.* **K, *Dhpr RNAi; Trh RNAi:*** *CgGal4 UAS-mitoGFP / UAS-Dhpr RNAi; UAS-Trh RNAi / +.* **L, *Dhpr RNAi; ple RNAi:*** *CgGal4 UAS-mitoGFP / UAS-Dhpr RNAi; UAS-ple RNAi / +.* **M, *Dhpr RNAi;***

Pu RNAi; UAS-Drp1: *CgGal4 UAS-mitoGFP / UAS-Dhpr RNAi; UAS-Pu RNAi / UAS-Drp1.* **N, *Dhpr RNAi; Nos RNAi; UAS-Drp1:*** *CgGal4 UAS-mitoGFP / UAS-Dhpr RNAi; UAS-Nos RNAi / UAS-Drp1.*

Fig. S9 A, *CTRL:* *CgGal4 UAS-mitoGFP / +; UAS-attp2 / +.* **B, *Dhpr RNAi:*** *CgGal4 UAS-mitoGFP / UAS-Dhpr RNAi.* **C, *Marf RNAi:*** *CgGal4 UAS-mitoGFP / +; UAS-Marf RNAi / +.* **D, *Opa1 RNAi:*** *CgGal4 UAS-mitoGFP / +; UAS-Opa1 RNAi / +.* **E, *Dhpr RNAi; Marf RNAi:*** *CgGal4 UAS-mitoGFP / UAS-Dhpr RNAi; UAS-Marf RNAi / +.* **F, *Dhpr RNAi; Opa1 RNAi:*** *CgGal4 UAS-mitoGFP / UAS-Dhpr RNAi; UAS-Opa1 RNAi / +.* **G, *Marf-myc OE:*** *CgGal4 UAS-mitoGFP/ UAS-Marf-myc.* **H, *Dhpr RNAi; Marf-myc OE:*** *CgGal4 UAS-mitoGFP UAS-Marf-myc/ UAS-Dhpr RNAi.* **I, *Drp1 RNAi:*** *CgGal4 UAS-mitoGFP/ UAS-Drp1 RNAi.* **J, *Dhpr RNAi; Drp1 RNAi:*** *CgGal4 UAS-mitoGFP UAS-Drp1 RNAi / UAS-Dhpr RNAi.*

Figure S1

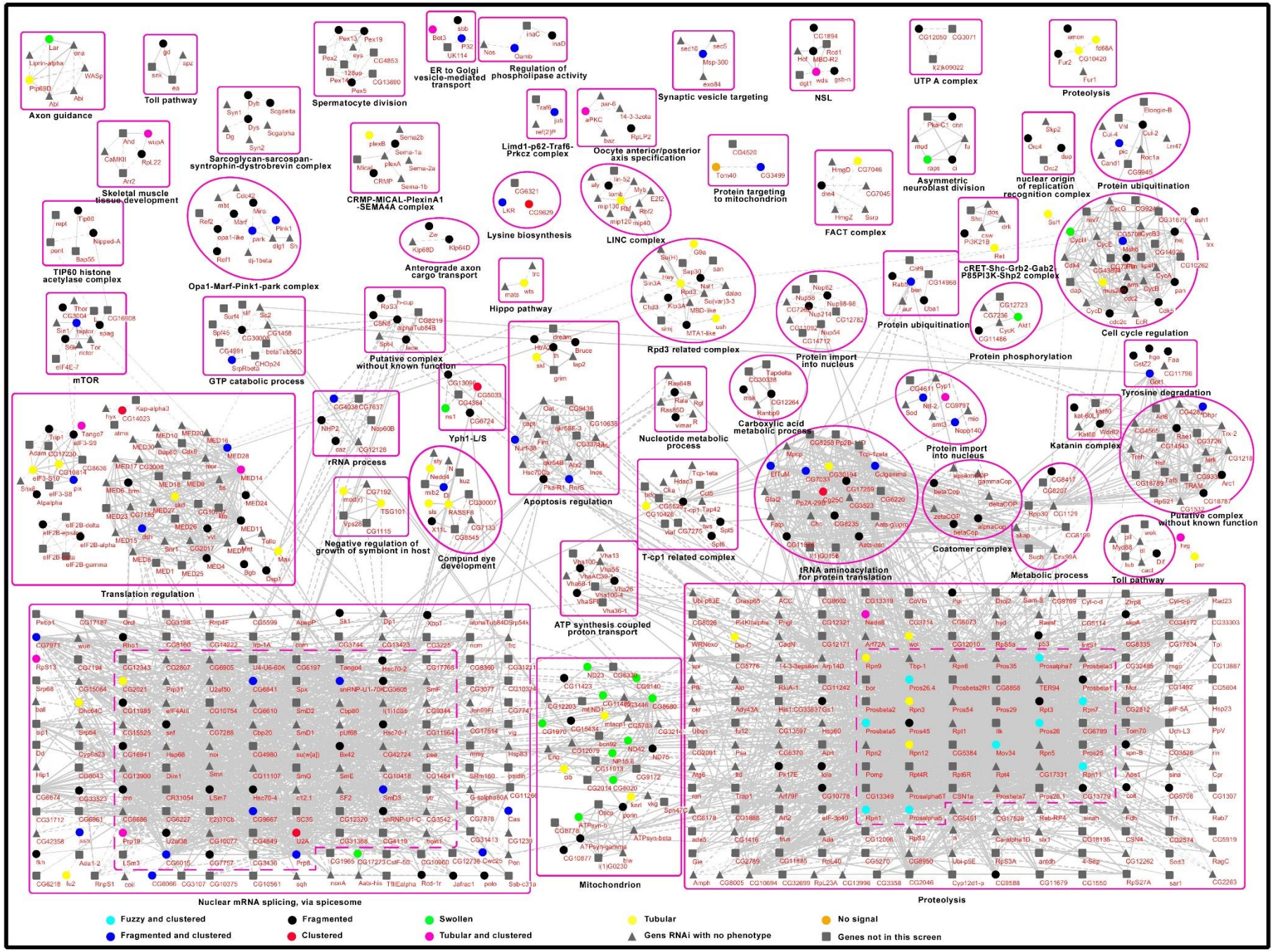
Axon guidance
Toll pathway
Sarcoglycan-sarcospan-syntrophin-dystrobrevin complex
Skeletal muscle tissue development
Spermatocyte division
CRMP-MICAL-PlexinA1-SEMA4A complex
ER to Golgi vesicle-mediated transport
Regulation of phospholipase activity
Limd1-p62-Traf6-Prkcz complex
Oocyte anterior/posterior axis specification
Lysine biosynthesis
LINC complex
Anterograde axon cargo transport
Hippo pathway
Synaptic vesicle targeting
NSL
UTP A complex
Proteolysis
Asymmetric neuroblast division
nuclear origin of replication recognition complex
Protein ubiquitination
Protein targeting to mitochondrion
FACT complex
cRET-Shc-Grb2-Gab2 P85PI3K-Shp2 complex
Cell cycle regulation
TIP60 histone acetylase complex
Opa1-Marf-Pink1-park complex
mTOR
GTP catabolic process
Putative complex without known function
Rpd3 related complex
Protein import into nucleus
Protein phosphorylation
Tyrosine degradation
Carboxylic acid metabolic process
Katanin complex
Yph1-L/S
rRNA process
Nucleotide metabolic process
Apoptosis regulation
Translation regulation
Negative regulation of growth of symbiont in host
Compound eye development
T-cp1 related complex
tRNA aminoacylation for protein translation
Coatomer complex
Metabolic process
ATP synthesis coupled proton transport
Nuclear mRNA splicing, via spicesome
Mitochondrion
Proteolysis
Fuzzy and clustered
Fragmented and clustered
Fragmented
Clustered
Swollen
Tubular and clustered
Tubular
Gens RNAi with no phenotype
No signal
Genes not in this screen

Fig. S1. **The complex analysis of the hits from the mitochondrial morphology screening.** The different phenotypes of the mitochondria are color coded and indicated at the bottom of the figure.

Figure S2

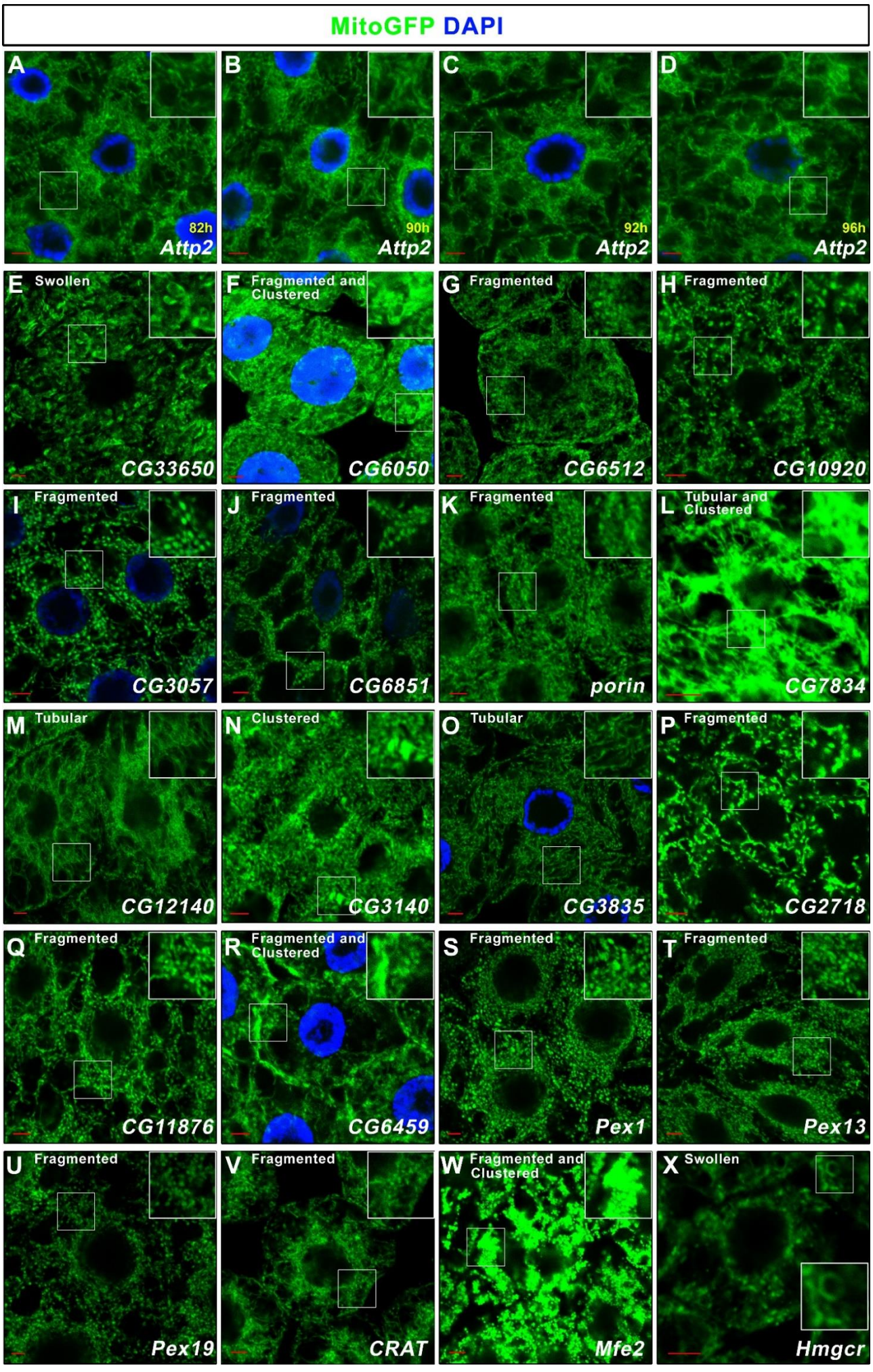
MitoGFP DAPI
A
82h
Attp2
B
90h
Attp2
C
92h
Attp2
D
96h
Attp2
E Swollen
CG33650
F Fragmented and Clustered
CG6050
G Fragmented
CG6512
H Fragmented
CG10920
I Fragmented
CG3057
J Fragmented
CG6851
K Fragmented
porin
L Tubular and Clustered
CG7834
M Tubular
CG12140
N Clustered
CG3140
O Tubular
CG3835
P Fragmented
CG2718
Q Fragmented
CG11876
R Fragmented and Clustered
CG6459
S Fragmented
Pex1
T Fragmented
Pex13
U Fragmented
Pex19
V Fragmented
CRAT
W Fragmented and Clustered
Mfe2
X Swollen
Hmgcr

Fig. S2. The mitochondrial morphology in the fat body tissues with indicated gene RNAi is shown. All these genes that had been mentioned in the main text but did not shown in the main figures were shown here. The boxed region in each image was enlarged in the inset to show the typical mitochondrial morphology. The phenotype category for each genotype is listed on the top of image. In **A-D,** the ages of larvae were labeled. The mitochondria were labeled by mitoGFP (green) and the nuclei were labeled by DAPI (blue). The scale bars are 5μm.

Figure S3

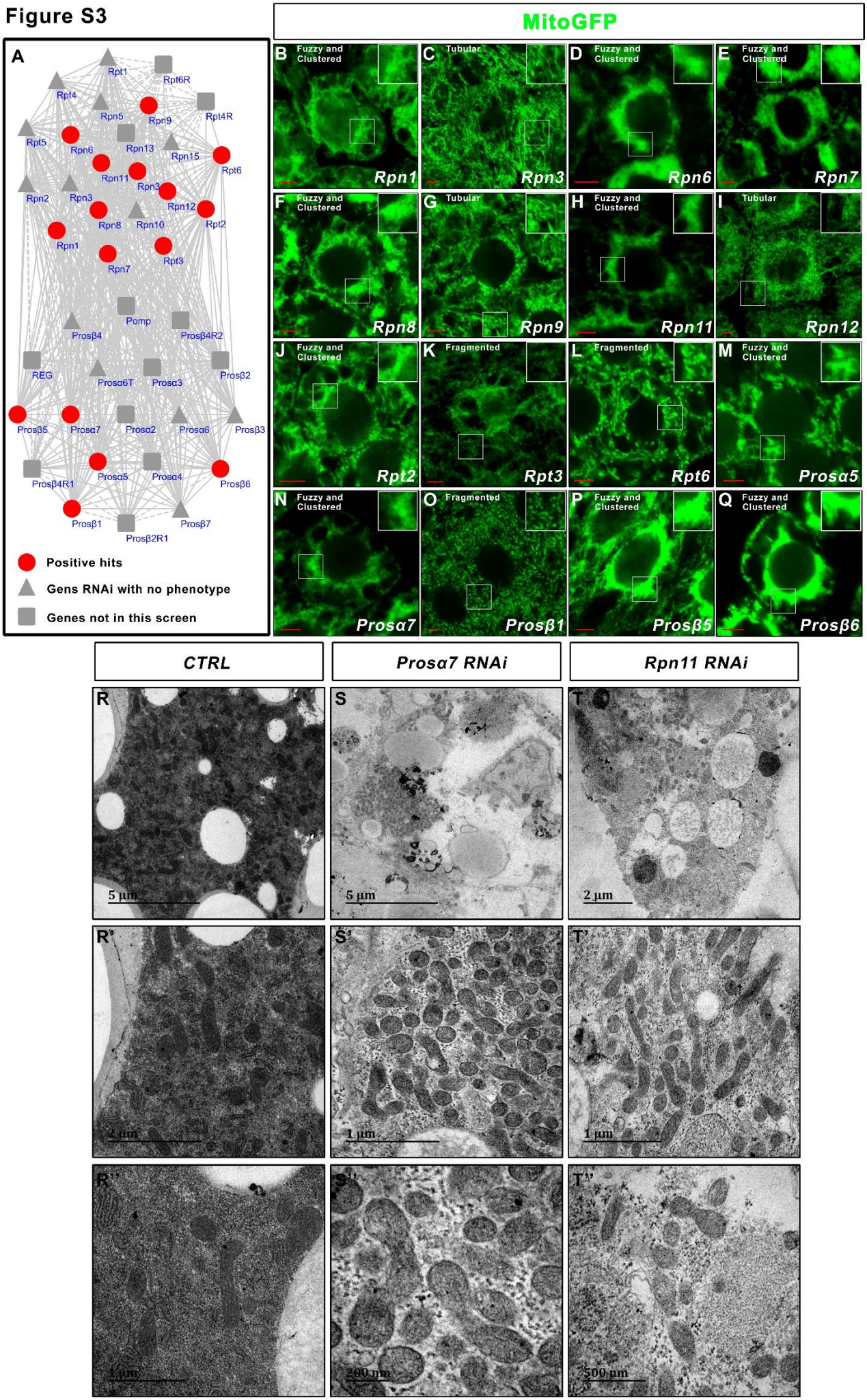
A
Rpt1
Rpt6R
Rpt4
Rpn5
Rpn9
Rpt4R
Rpt5
Rpn6
Rpn13
Rpn15
Rpt6
Rpn11
Rpn3
Rpn2
Rpn3
Rpn12
Rpn8
Rpn10
Rpt2
Rpn1
Rpt3
Rpn7
Pomp
Prosβ4
Prosβ4R2
REG
Prosα6T
Prosα3
Prosβ2
Prosβ5
Prosα7
Prosα2
Prosα6
Prosβ3
Prosβ4R1
Prosα5
Prosα4
Prosβ6
Prosβ1
Prosβ7
Prosβ2R1
Positive hits
Gens RNAi with no phenotype
Genes not in this screen
MitoGFP
B Fuzzy and Clustered Rpn1
C Tubular Rpn3
D Fuzzy and Clustered Rpn6
E Fuzzy and Clustered Rpn7
F Fuzzy and Clustered Rpn8
G Tubular Rpn9
H Fuzzy and Clustered Rpn11
I Tubular Rpn12
J Fuzzy and Clustered Rpt2
K Fragmented Rpt3
L Fragmented Rpt6
M Fuzzy and Clustered Prosα5
N Fuzzy and Clustered Prosα7
O Fragmented Prosβ1
P Fuzzy and Clustered Prosβ5
Q Fuzzy and Clustered Prosβ6
CTRL
Prosα7 RNAi
Rpn11 RNAi
R
S
T
5 µm
5 µm
2 µm
R'
S'
T'
2 µm
1 µm
1 µm
R''
S''
T''
1 µm
200 nm
500 nm

Fig. S3. Sixteen genes encoding proteasome components were identified in this mitochondrial morphology screening. A. A scheme to show that the proteasome components that had been identified in this screening. **B-Q.** The mitochondrial morphology in the fat body cells with indicated gene knocked down. Mitochondria were labeled with mitoGFP (green) and the nuclei were labeled with DAPI staining (blue). The boxed region in each image was enlarged in the inset to show the typical mitochondrial morphology. The phenotype category for each genotype was listed on the top of image. The scale bars are 5μm. **R-T"**. The TEM of the fat body tissues with indicated gene knocked down. The scale bars are as indicated. 3 different scales were shown for each genotype.

Figure S4

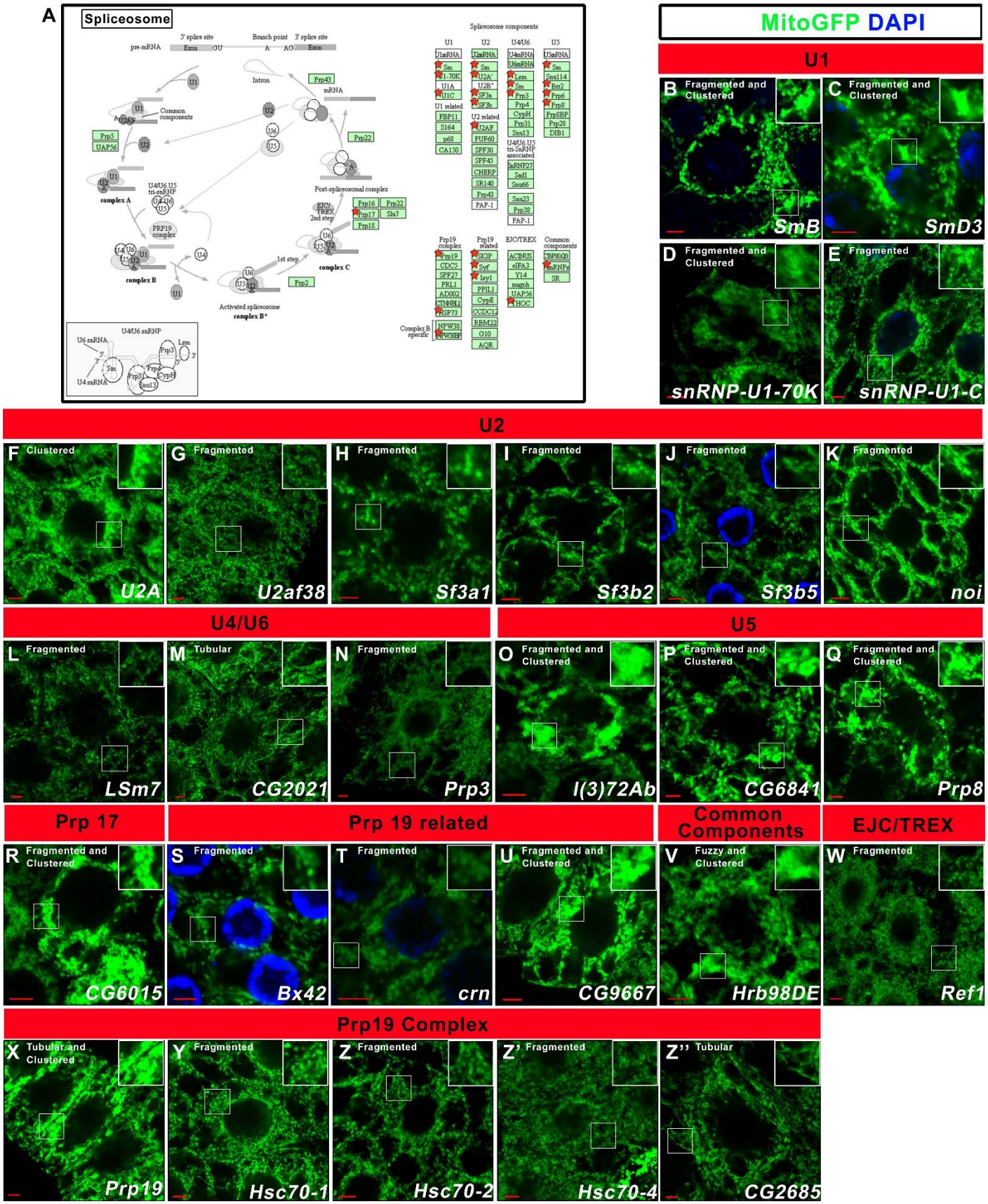
A
Spliceosome
MitoGFP DAPI
U1
B Fragmented and Clustered
SmB
C Fragmented and Clustered
SmD3
D Fragmented and Clustered
snRNP-U1-70K
E Fragmented
snRNP-U1-C
U2
F Clustered
U2A
G Fragmented
U2af38
H Fragmented
Sf3a1
I Fragmented
Sf3b2
J Fragmented
Sf3b5
K Fragmented
noi
U4/U6
U5
L Fragmented
LSm7
M Tubular
CG2021
N Fragmented
Prp3
O Fragmented and Clustered
l(3)72Ab
P Fragmented and Clustered
CG6841
Q Fragmented and Clustered
Prp8
Prp 17
Prp 19 related
Common Components
EJC/TREX
R Fragmented and Clustered
CG6015
S Fragmented
Bx42
T Fragmented
crn
U Fragmented and Clustered
CG9667
V Fuzzy and Clustered
Hrb98DE
W Fragmented
Ref1
Prp19 Complex
X Tubular and Clustered
Prp19
Y Fragmented
Hsc70-1
Z Fragmented
Hsc70-2
Z' Fragmented
Hsc70-4
Z'' Tubular
CG2685

Fig. S4. Twenty-seven genes encoding spliceosome components were identified in this mitochondrial morphology screening. A. The spliceosome components and their functional pathway were shown (adapted from KEGG). The components identified in this screening were labeled with red stars. **B-Z"**. The mitochondrial morphology in the fat body cells with indicated gene RNAi were shown. The name of the subcomplex that the proteins encoded by the identified genes belong to were labeled on the top of the images. The mitochondria were labeled by mitoGFP (green) and the nuclei were labeled by DAPI (blue). The boxed region in each image was enlarged in the inset to show the typical mitochondrial morphology. The phenotype category for each genotype was listed on the top of image. The scale bars are 5μm.

Figure S5

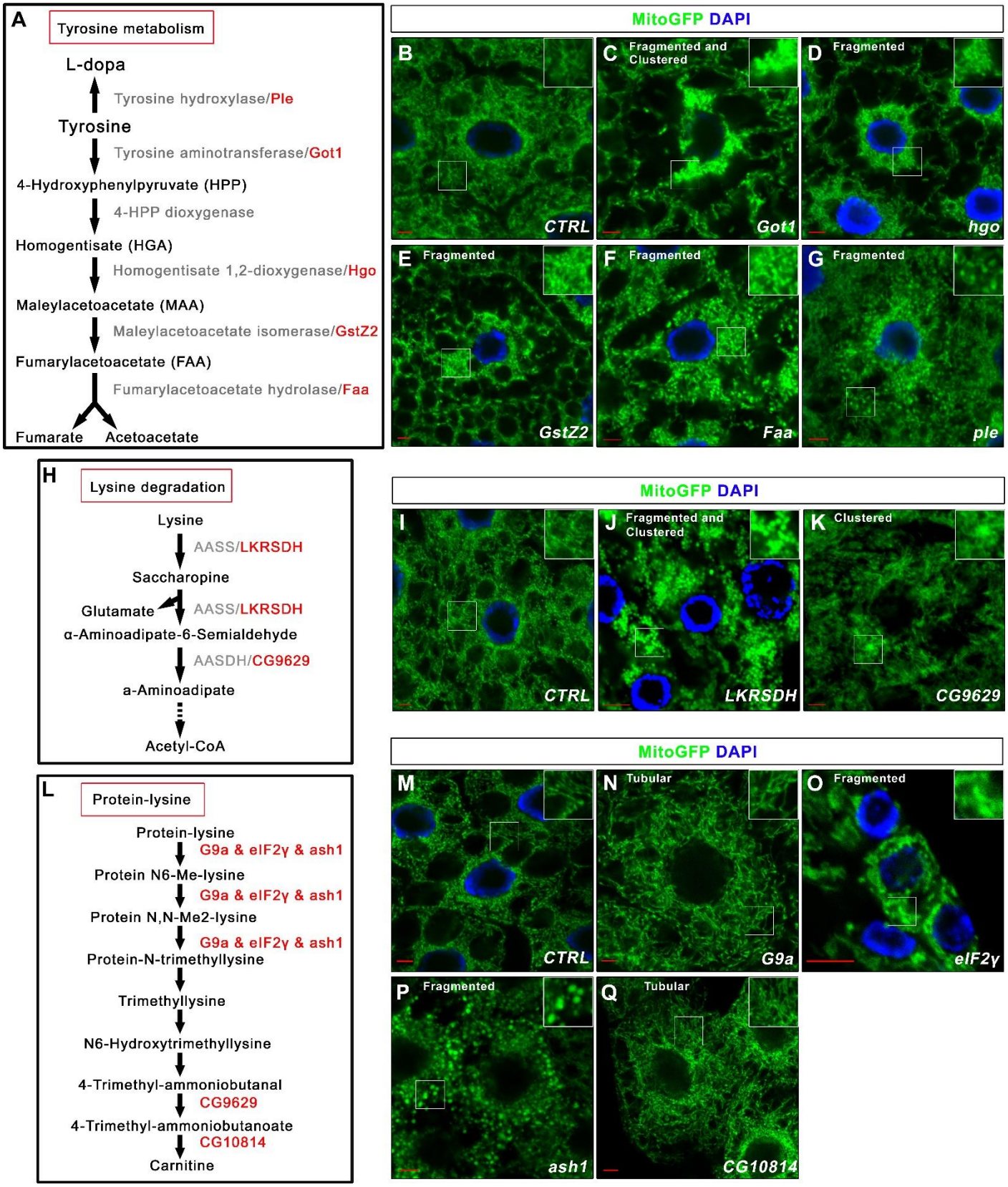
A
Tyrosine metabolism
L-dopa
Tyrosine hydroxylase/Ple
Tyrosine
Tyrosine aminotransferase/Got1
4-Hydroxyphenylpyruvate (HPP)
4-HPP dioxygenase
Homogentisate (HGA)
Homogentisate 1,2-dioxygenase/Hgo
Maleylacetoacetate (MAA)
Maleylacetoacetate isomerase/GstZ2
Fumarylacetoacetate (FAA)
Fumarylacetoacetate hydrolase/Faa
Fumarate
Acetoacetate
MitoGFP DAPI
B
CTRL
C
Fragmented and Clustered
Got1
D
Fragmented
hgo
E
Fragmented
GstZ2
F
Fragmented
Faa
G
Fragmented
ple
H
Lysine degradation
Lysine
AASS/LKRSDH
Saccharopine
Glutamate
AASS/LKRSDH
α-Aminoadipate-6-Semialdehyde
AASDH/CG9629
a-Aminoadipate
Acetyl-CoA
MitoGFP DAPI
I
CTRL
J
Fragmented and Clustered
LKRSDH
K
Clustered
CG9629
L
Protein-lysine
Protein-lysine
G9a & eIF2γ & ash1
Protein N6-Me-lysine
G9a & eIF2γ & ash1
Protein N,N-Me2-lysine
G9a & eIF2γ & ash1
Protein-N-trimethyllysine
Trimethyllysine
N6-Hydroxytrimethyllysine
4-Trimethyl-ammoniobutanal
CG9629
4-Trimethyl-ammoniobutanoate
CG10814
Carnitine
MitoGFP DAPI
M
CTRL
N
Tubular
G9a
O
Fragmented
eIF2γ
P
Fragmented
ash1
Q
Tubular
CG10814

Fig. S5. The reduction of the enzymes involved in tyrosine and lysine metabolism led to abnormal mitochondrial morphology. A. A scheme showed the key enzymes involved in tyrosine metabolism. **B-G**. The mitochondria became fragmented and sometimes clustered when the expression of the indicated genes was reduced. **H.** A scheme showed the key enzymes in the lysine degradation pathway. **I-K**. The mitochondrial morphology was abnormal when *LKRSDH* and *CG9629* were knocked down. **L.** A scheme showed the enzymes required for protein lysine residue methylation process and the enzymes that synthesis carnitine from tri-methyllysine. **M-Q.** The mitochondrial morphology was abnormal when the indicated genes were knocked down in fat body tissues. The red label in **A**, **H**, and **L** indicates the fly genes encoding the indicated enzymes that had been identified in this screen. In **B-G**, **I-K**, and **M-Q,** the green signals were mitoGFP signals to indicate mitochondrial morphology and the blue signals were DAPI staining to indicate the nuclei. The scale bars are 5μm. The boxed region in each image was enlarged and shown in the inset to present the typical mitochondrial morphology. The phenotype category for each genotype was listed on the top of image.

Figure S6

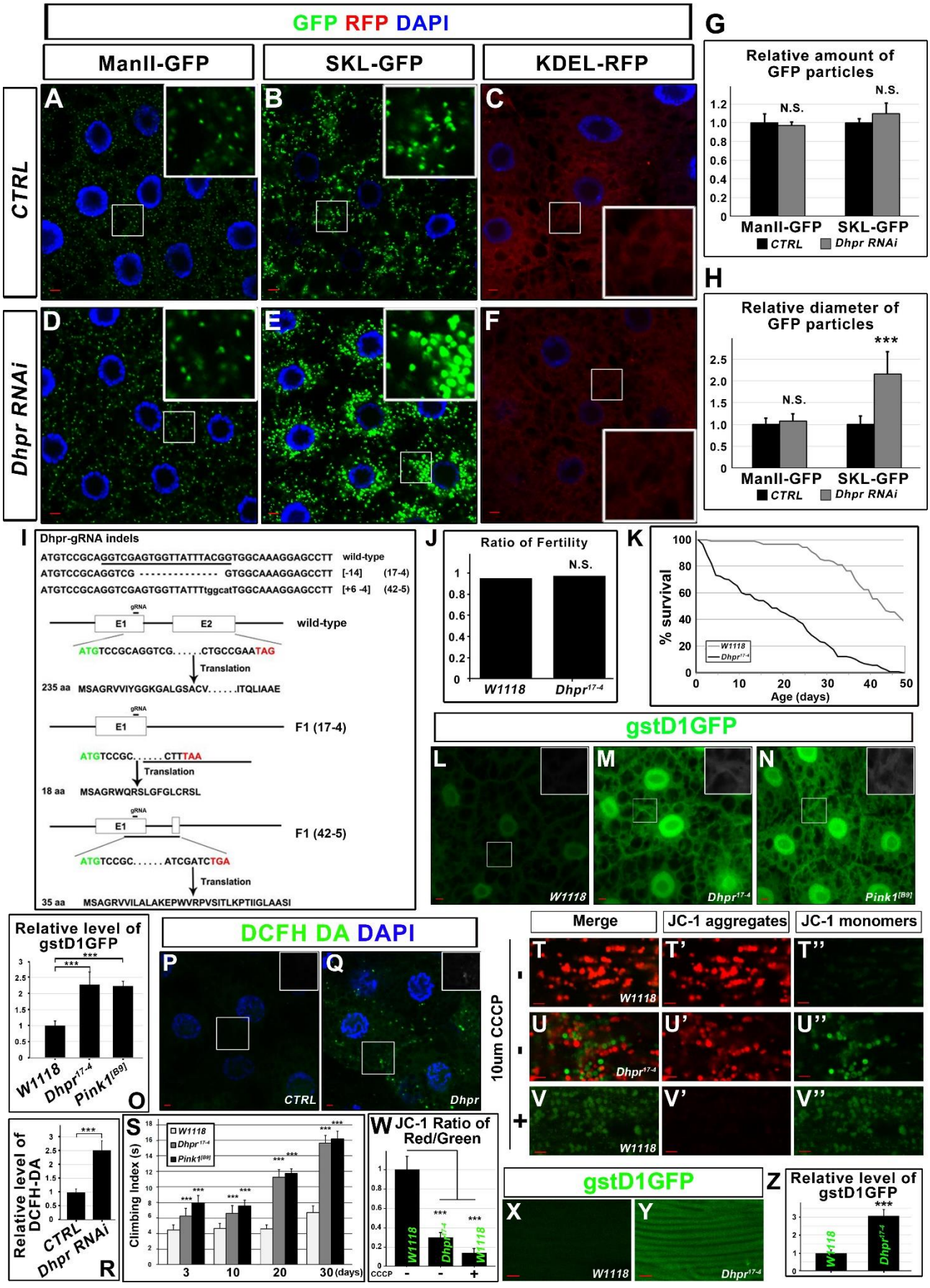
GFP RFP DAPI
ManII-GFP
SKL-GFP
KDEL-RFP
CTRL
Dhpr RNAi
A
B
C
D
E
F
G
Relative amount of GFP particles
N.S.
N.S.
ManII-GFP
SKL-GFP
CTRL
Dhpr RNAi
H
Relative diameter of GFP particles
***
N.S.
ManII-GFP
SKL-GFP
CTRL
Dhpr RNAi
I
Dhpr-gRNA indels
ATGTCCGCAGGTCGAGTGGTTATTTACGGTGGCAAAGGAGCCTT wild-type
ATGTCCGCAGGTCG ---------- GTGGCAAAGGAGCCTT [-14] (17-4)
ATGTCCGCAGGTCGAGTGGTTATTTtggcatTGGCAAAGGAGCCTT [+6 -4] (42-5)
gRNA
E1
E2
wild-type
ATGTCCGCAGGTCG.....CTGCCGAATAG
Translation
235 aa MSAGRVVIYGGKGALGSACV.....ITQLIAAE
F1 (17-4)
ATGTCCGC.....CTTTAA
18 aa MSAGRWQRSLGFGLCRSL
F1 (42-5)
ATGTCCGC.....ATCGATCTGA
35 aa MSAGRVVILALAKEPWVRPVSITLKPTIIGLAASI
J
Ratio of Fertility
N.S.
W1118
Dhpr17-4
K
% survival
Age (days)
W1118
Dhpr17-4
gstD1GFP
L
M
N
W1118
Dhpr17-4
Pink1[B9]
Relative level of gstD1GFP
W1118
Dhpr17-4
Pink1[B9]
O
DCFH DA DAPI
P
Q
CTRL
Dhpr
Merge
JC-1 aggregates
JC-1 monomers
10um CCCP
T
T'
T''
U
U'
U''
V
V'
V''
W1118
Dhpr17-4
W1118
Relative level of DCFH-DA
CTRL
Dhpr RNAi
R
S
Climbing Index (s)
W1118
Dhpr17-4
Pink1[B9]
3
10
20
30 (days)
W
JC-1 Ratio of Red/Green
CCCP
gstD1GFP
X
Y
W1118
Dhpr17-4
Z
Relative level of gstD1GFP
W1118
Dhpr17-4

Fig. S6. Loss of *Dhpr* leads to the reduction of life span and increase of the ROS production. A-H. The patterns of Golgi (ManII-GFP), peroxisomes (SKL-GFP), and ER (KDEL-RFP) were analyzed in fat body tissues of indicated genotypes. The patterns of Golgi and ER markers were similar in *Dhpr* RNAi and control fat body tissues. SKL-GFP labeled peroxisomes puncta were larger in *Dhpr* RNAi tissues than in the control tissues. The boxed region in each image was enlarged in the inset. **G.** is the quantification of the numbers of the particles in **A, B, D,** and **E**. n = 3 images for each genotype; N.S., not significant; two-tailed unpaired student t-test. **H.** is the quantification of the relative particle size in **A, B, D,** and **E**. n = 3 images for each genotype; N.S., not significant. ***, $p < 0.001$; two-tailed unpaired student t-test. **I.** The scheme showed the CRISPR/Cas9 mediated knock out strategy and the isolated alleles. Homozygous $Dhpr^{17-4}$ and $Dhpr^{42-5}$ mutant alleles were analyzed and the data of $Dhpr^{17-4}$ allele were presented. **J.** $Dhpr^{17-4}$ mutant flies were fertile. n = 3 replicates, 50 flies per replicate; N.S., not significant; two-tailed unpaired student t-test. **K.** $Dhpr^{17-4}$ mutant flies have reduced life span. The male flies were analyzed. $p < 0.0001$, log rank test; n = 100 flies. **L-N.** *gstD1*GFP reporter (green) shows that $Dhpr^{17-4}$ and $Pink1^{[B9]}$ third *instar* larvae fat body tissues have elevated ROS production. **O.** is the quantification of the relative level of gstD1 GFP in **L-N.** n = 3 images for each genotype; ***, $p < 0.001$; one-way ANOVA/Bonferroni's multiple comparisons test. **P, Q.** DCFH DA staining shows that *Dhpr* RNAi in the fat body tissues leads to increased ROS production. **R.** is the quantification of the relative level of DCFH-DA in **P** and **Q.** n = 3 images for each genotype; ***, $p < 0.001$; two-tailed unpaired student t-test. **S.** The climbing index indicates that *Dhpr* and *Pink1* mutants have gradually reduced climbing ability with aging. n = 3 - 10 vials per genotype, 10 flies for each vial; ***, $p < 0.001$; one-way ANOVA/Bonferroni's multiple comparisons test. **T-V.** JC-1 staining showed that $Dhpr^{17-4}$ flight muscle tissues from 15-day-old flies have low mitochondrial transmembrane potential ($\Delta\Psi m$). Red fluorescence (JC-1 aggregate) indicates healthy mitochondria, while green fluorescence (JC-1 monomers) indicates inactive mitochondria without $\Delta\Psi m$. **W.** is the quantification of JC-1 staining in **T-V**. n = 3 images for each genotype; ***, $p < 0.001$; one-way ANOVA/Bonferroni's multiple comparisons test. **X, Y.** *gstD1GFP* reporter (green) showed that *Dhpr17-4* flight muscle tissues from 15-day-old flies have elevated ROS production. **Z.** is the quantification of the relative level of gstD1 GFP in **X** and **Y**. n = 3 images for each genotype; ***, $p < 0.001$; two-tailed unpaired t-test. The scale bars in IF images are 5μm.

Figure S7

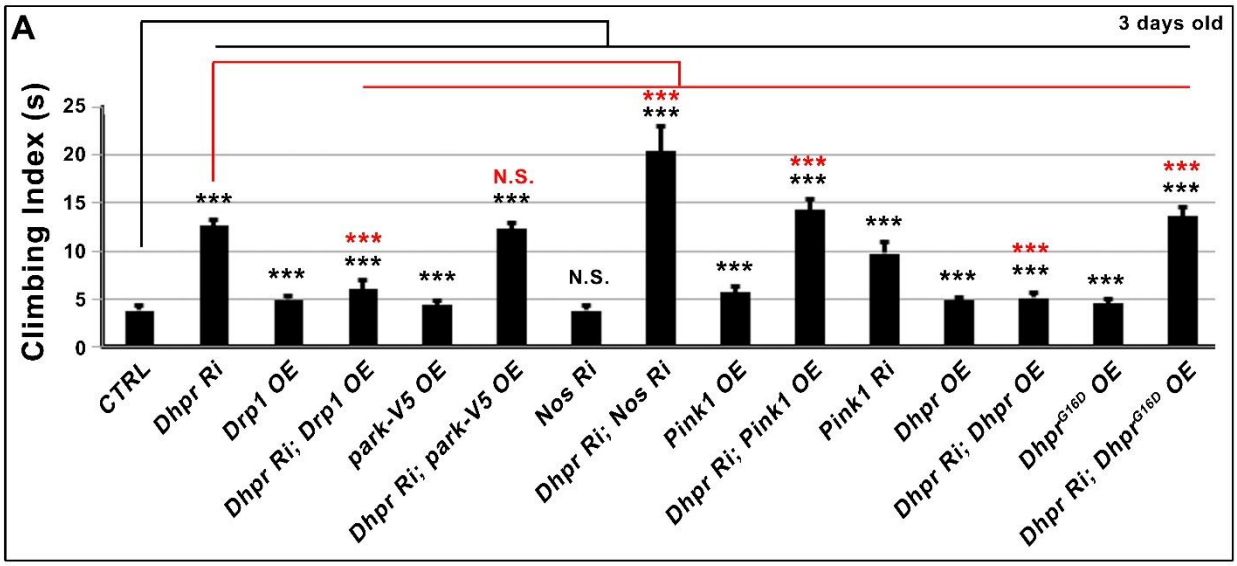
A
3 days old
Climbing Index (s)
25
20
15
10
5
0
***
N.S.
CTRL
Dhpr Ri
Drp1 OE
Dhpr Ri; Drp1 OE
park-V5 OE
Dhpr Ri; park-V5 OE
Nos Ri
Dhpr Ri; Nos Ri
Pink1 OE
Dhpr Ri; Pink1 OE
Pink1 Ri
Dhpr OE
Dhpr Ri; Dhpr OE
DhprG16D OE
Dhpr Ri; DhprG16D OE

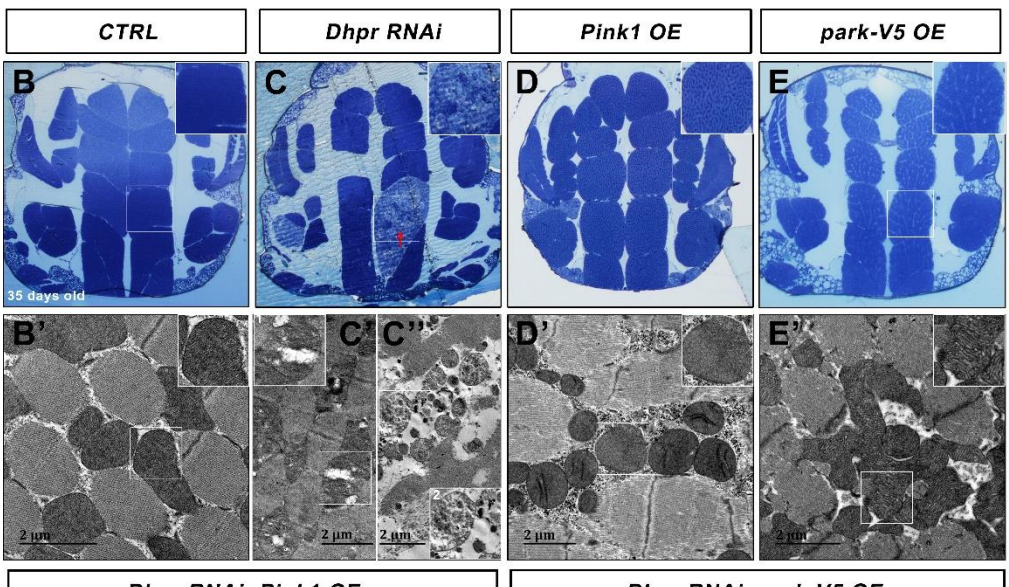
CTRL
Dhpr RNAi
Pink1 OE
park-V5 OE
B
C
D
E
35 days old
B'
C'
C''
D'
E'
2 µm

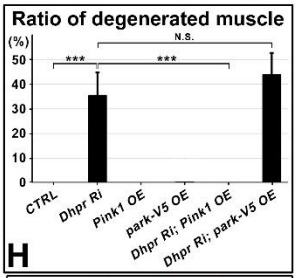
Ratio of degenerated muscle
(%)
50
40
30
20
10
0
***
N.S.
CTRL
Dhpr Ri
Pink1 OE
park-V5 OE
Dhpr Ri; Pink1 OE
Dhpr Ri; park-V5 OE
H

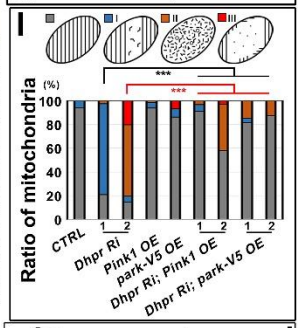
I
Ratio of mitochondria
(%)
100
80
60
40
20
0
***
CTRL
Dhpr Ri
Pink1 OE
park-V5 OE
Dhpr Ri; Pink1 OE
Dhpr Ri; park-V5 OE

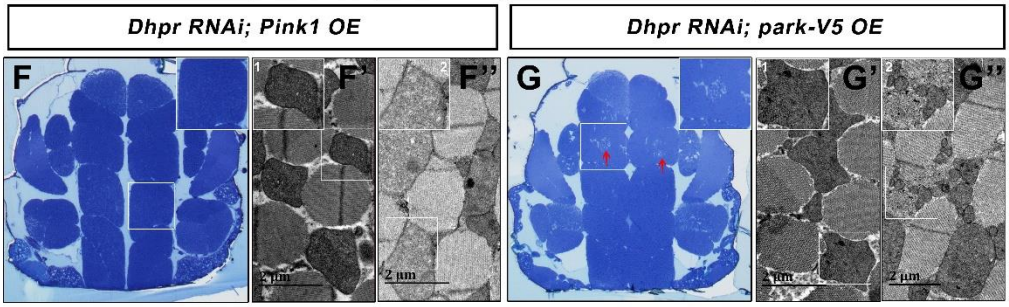
Dhpr RNAi; Pink1 OE
Dhpr RNAi; park-V5 OE
F
F'
F''
G
G'
G''
2 µm

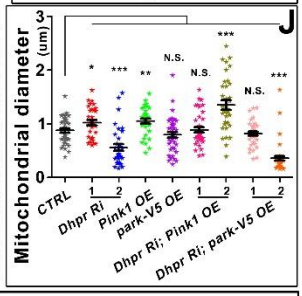
J
Mitochondrial diameter (um)
3
2
1
0
*
***
**
N.S.
CTRL
Dhpr Ri
Pink1 OE
park-V5 OE
Dhpr Ri; Pink1 OE
Dhpr Ri; park-V5 OE

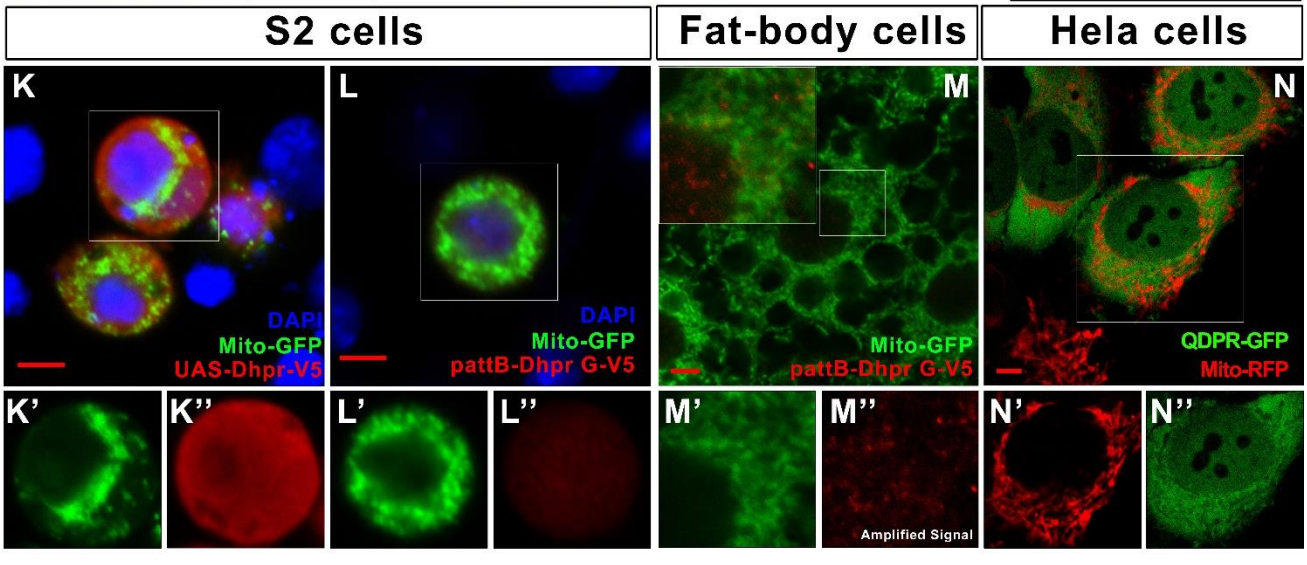
S2 cells
Fat-body cells
Hela cells
K
L
M
N
DAPI
Mito-GFP
UAS-Dhpr-V5
pattB-Dhpr G-V5
QDPR-GFP
Mito-RFP
K'
K''
L'
L''
M'
M''
N'
N''
Amplified Signal

Fig. S7. The overexpression of *Pink1* or *park* partially rescues muscle defects caused by *Dhpr* RNAi. A. The climbing index of the 3-day-old adult flies with indicated genotypes. Muscle specific knockdown of *Dhpr* led to decreased climbing ability and *Pink1*, *park* overexpression could not rescue the mobility defects caused by *Dhpr* RNAi. *Nos* RNAi enhanced the climbing defects caused by *Dhpr* RNAi. The wild type but not the G16D mutant form of *Dhpr* could rescue the climbing defects caused by *Dhpr* RNAi. Ri, RNAi; OE, overexpression. n = 3 - 10 vials per genotype,10 flies per vial; N.S., not significant; ***, $p < 0.001$; one-way ANOVA/Bonferroni's multiple comparisons test. **B-G.** are the toluidine blue staining of the fly thorax thick sections from 35-day-old flies with indicated genotypes. The boxed regions were enlarged in the insets to show detailed phenotypes of the muscle fragments. **B'-G"** are the TEM images of thorax thin sections to show the detailed morphology of mitochondria and muscle fibers. The scale bars are as indicated. **H.** is the quantification of the ratio of degenerated muscle fragments in **B-G**. Ri, RNAi*;* OE, overexpression. n = 3 - 6; N.S, not significant; ***, $P<0.001$; one-way ANOVA/Bonferroni's multiple comparisons test. **I.** is the quantification of the ratio of mitochondria in **B'-G"**. The diagram on top of this panel shows the typical normal mitochondria (grey) and abnormal mitochondria. The abnormal mitochondria were categorized into three type based on cristae morphology. Type I (blue): mitochondria lose some cristae and there are obvious empty spaces between tightly packed cristae. Type II (orange): the cristae of the mitochondria are disorganized and loose. Type III (red): mitochondria lose most of its cristae, more than half of the mitochondria area was empty. Ri, RNAi*;* OE, overexpression. n = 3 images for each genotype; ***, $p < 0.001$; Chi-square (and Fisher's exact) test. **J.** is the quantification of the mitochondrial diameters in **B'-G"**. Ri, RNAi*;* OE, overexpression. n = 27; N.S, not significant; *, $p < 0.05$; **, $p < 0.01$; ***, $p < 0.001$; one-way ANOVA/Bonferroni's multiple comparisons test. **K-N".** Dhpr is an evolutionary conserved cytosolic protein. **K-K"**. In S2 cells, overexpressed V5 tagged Dhpr is diffusely distributed inside the cytosol. MitoGFP (green) labels mitochondria, anti-V5 (red) indicate overexpressed Dhpr. DAPI (blue) labels the nucleus. **L-L".** Endogenous level of Dhpr expression shows a diffused pattern inside S2 cells. The genomic fragment contain a V5 tagged (C-terminal tag) Dhpr was introduced into S2 cells. MitoGFP (green) labels mitochondria, anti-V5 (red) indicate overexpressed Dhpr. DAPI (blue) labels the nucleus. **M-M"**. Endogenous level of Dhpr expression shows a diffused pattern in fat body tissues. The genomic fragment contain a V5 tagged (C-terminal tag) Dhpr was introduced into wide type flies. MitoGFP (green) labels mitochondria, anti-V5 (red) indicate overexpressed Dhpr. **N-N"**GFP tagged QDPR overexpression shows diffused pattern in Hela cells. MitoRFP (red) labels mitochondria and GFP (green) signals indicate QDPR distribution. The scale bars in the IF images are 5μm. The scale bars in the TEM images are as indicated.

Figure S8

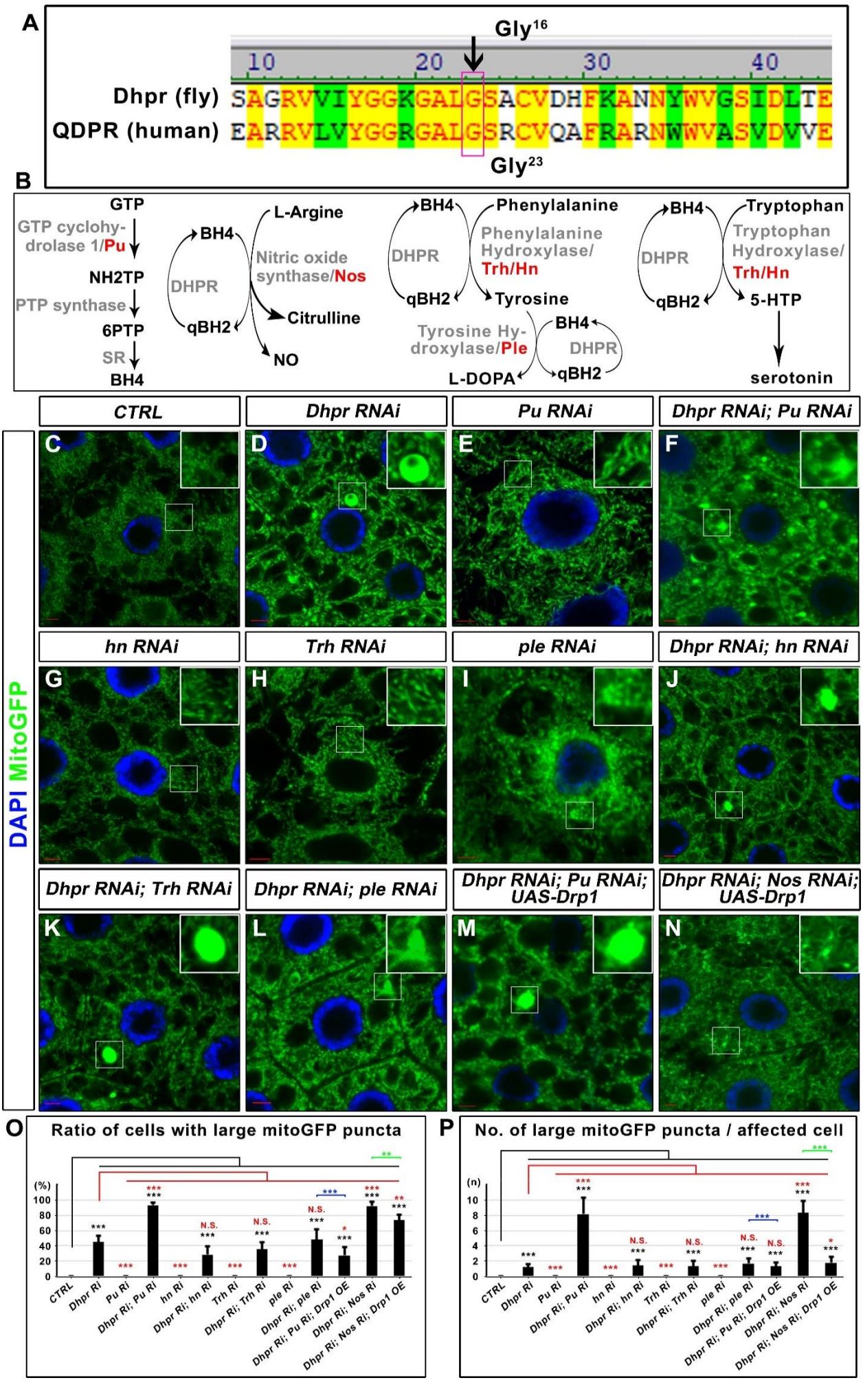
A
Gly16
10
20
30
40
Dhpr (fly) SAGRVVIYGGKGALGSACVDHFKANNYWVGSIDLTE
QDPR (human) EARRVLVYGGRGALGSRCVQAFRARNWWVASVDVVE
Gly23
B
GTP
GTP cyclohydrolase 1/Pu
NH2TP
PTP synthase
6PTP
SR
BH4
BH4
DHPR
qBH2
L-Argine
Nitric oxide synthase/Nos
Citrulline
NO
BH4
DHPR
qBH2
Phenylalanine
Phenylalanine Hydroxylase/ Trh/Hn
Tyrosine
Tyrosine Hydroxylase/Ple
L-DOPA
BH4
DHPR
qBH2
BH4
DHPR
qBH2
Tryptophan
Tryptophan Hydroxylase/ Trh/Hn
5-HTP
serotonin
CTRL
Dhpr RNAi
Pu RNAi
Dhpr RNAi; Pu RNAi
C
D
E
F
hn RNAi
Trh RNAi
ple RNAi
Dhpr RNAi; hn RNAi
G
H
I
J
DAPI MitoGFP
Dhpr RNAi; Trh RNAi
Dhpr RNAi; ple RNAi
Dhpr RNAi; Pu RNAi; UAS-Drp1
Dhpr RNAi; Nos RNAi; UAS-Drp1
K
L
M
N
O
Ratio of cells with large mitoGFP puncta
(%)
100
80
60
40
20
0
CTRL
Dhpr Ri
Pu Ri
Dhpr Ri; Pu Ri
hn Ri
Dhpr Ri; hn Ri
Trh Ri
Dhpr Ri; Trh Ri
ple Ri
Dhpr Ri; ple Ri
Dhpr Ri; Pu Ri; Drp1 OE
Dhpr Ri; Nos Ri
Dhpr Ri; Nos Ri; Drp1 OE
N.S.
P
No. of large mitoGFP puncta / affected cell
(n)
10
8
6
4
2
0
CTRL
Dhpr Ri
Pu Ri
Dhpr Ri; Pu Ri
hn Ri
Dhpr Ri; hn Ri
Trh Ri
Dhpr Ri; Trh Ri
ple Ri
Dhpr Ri; ple Ri
Dhpr Ri; Pu Ri; Drp1 OE
Dhpr Ri; Nos Ri
Dhpr Ri; Nos Ri; Drp1 OE
N.S.

Fig. S8. The genetic interaction between *Dhpr* and genes whose products consume or produce BH4. A. The alignment of Dhpr and QDPR showed that glycine^{16} in Dhpr is corresponding to glycine^{23} in QDPR. **B.** A scheme to show that the enzyme activities of the indicated proteins using BH4 as cofactors. **C-F.** *Pu* RNAi did not cause obvious mitochondrial defects in wild type fat body tissues but greatly enhanced the mitochondrial defects in *Dhpr* RNAi fat body tissues. **G-I**. The RNAi of *hn, Trh or ple* alone did not have mitochondrial phenotypes similar with *Dhpr* RNAi. **J-L.** The RNAi of *hn, Trh or ple* could not enhance the mitochondrial defects caused by RNAi of *Dhpr.* **M.** *Drp1* overexpression could partially rescue the mitochondrial defects caused by *Dhpr* and *pu* double RNAi. **N.** *Drp1* overexpression could partially rescue the mitochondrial defects caused by *Dhpr* and *Nos* double RNAi. The mitochondrial morphology in the fat body cells with indicated gene knocked down. Mitochondria were labeled with mitoGFP (green) and the nuclei were labeled with DAPI staining (blue). The boxed region in each image was enlarged in the inset to show the typical mitochondrial morphology. The scale bars are 5μm. **O.** is the quantification of the ratio of cells with large mitoGFP puncta in the fat body tissues with indicated genotypes. Ri, RNAi*;* OE, overexpression. n = 5; N. S., not significant; **, $p < 0.01$; ***, $p < 0.001$; one-way ANOVA/Bonferroni's multiple comparisons test. **P.** is the quantification of the average number of large mitoGFP puncta per affected cell in the fat body tissues with indicated genotypes. Ri, RNAi*;* OE, overexpression. n = 10; N. S., not significant; **, $p < 0.01$; ***, $p < 0.001$; one-way ANOVA/Bonferroni's multiple comparisons test.

Figure S9

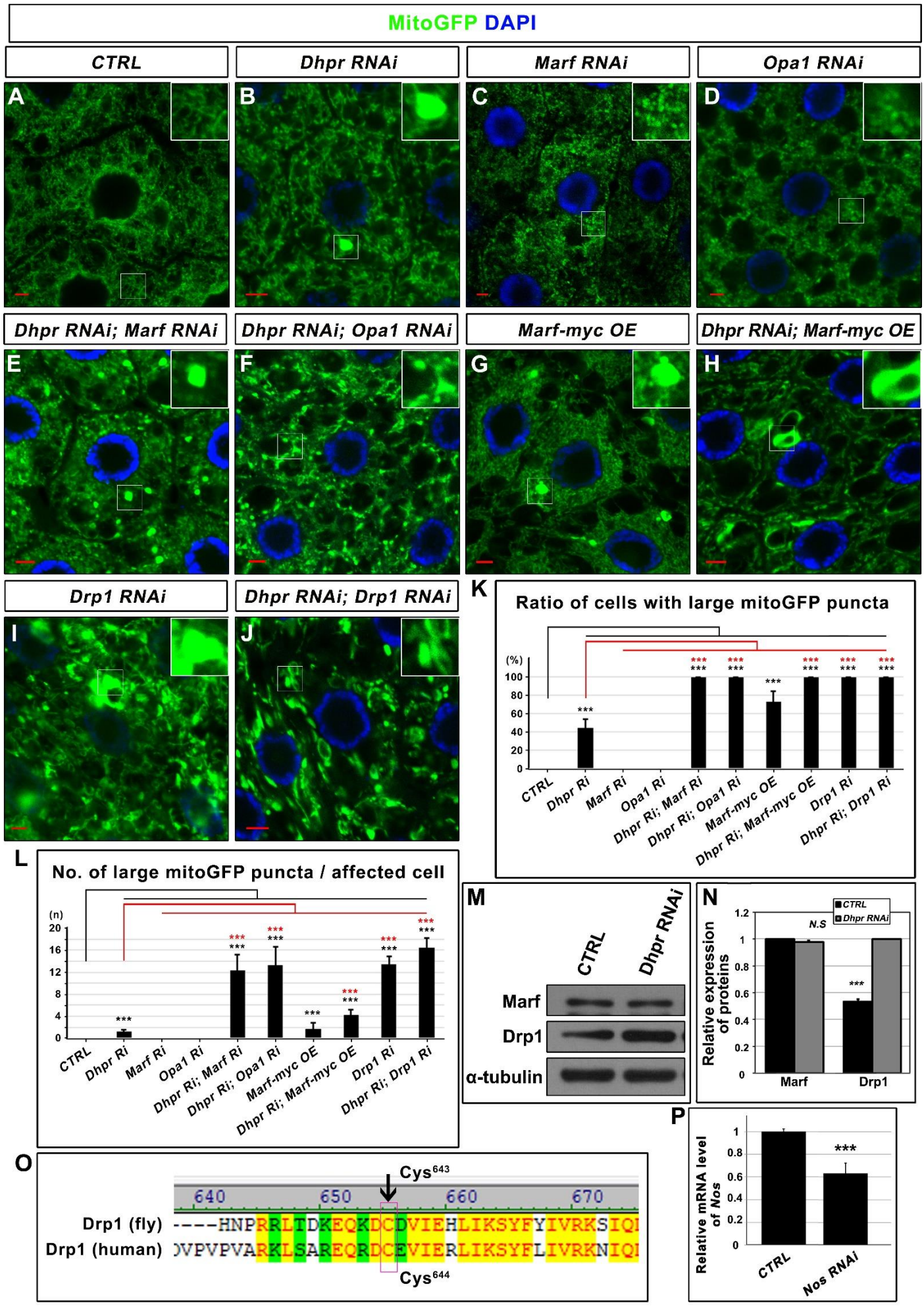
MitoGFP DAPI
CTRL
Dhpr RNAi
Marf RNAi
Opa1 RNAi
A
B
C
D
Dhpr RNAi; Marf RNAi
Dhpr RNAi; Opa1 RNAi
Marf-myc OE
Dhpr RNAi; Marf-myc OE
E
F
G
H
Drp1 RNAi
Dhpr RNAi; Drp1 RNAi
I
J
K
Ratio of cells with large mitoGFP puncta
(%)
CTRL
Dhpr Ri
Marf Ri
Opa1 Ri
Dhpr Ri; Marf Ri
Dhpr Ri; Opa1 Ri
Marf-myc OE
Dhpr Ri; Marf-myc OE
Drp1 Ri
Dhpr Ri; Drp1 Ri
L
No. of large mitoGFP puncta / affected cell
(n)
M
CTRL
Dhpr RNAi
Marf
Drp1
α-tubulin
N
CTRL
Dhpr RNAi
N.S
Relative expression of proteins
Marf
Drp1
O
Cys643
640
650
660
670
Drp1 (fly) ----HNPRRLTDKEQKDCDVIEHLIKSYFYIVRKSIQI
Drp1 (human))VPVPVARKLSARFQRDCEVIERLIKSYFLIVRKNIQI
Cys644
P
Relative mRNA level of Nos
CTRL
Nos RNAi

Fig. S9. The genetic interaction between *Dhpr* and other core machinery of mitochondrial fusion and fission. The mitochondrial morphology in the fat body cells with indicated gene knocked down. Mitochondria were labeled with mitoGFP (green) and the nuclei are labeled with DAPI staining (blue). The scale bars are 5μm. **A-J.** *Opa1* RNAi, *marf* RNAi, *marf* overexpression, and *Drp1* RNAi could modify the mitochondrial morphology defects caused by *Dhpr* RNAi. In these tissues, the mitochondrial defects were worse than that in *Dhpr* RNAi alone. **K.** The ratio of cells with large mitoGFP puncta in the fat body tissues with indicated genotypes. Ri, RNAi*;* OE, overexpression. n = 5; N. S., not significant; **, $p < 0.01$; ***, $p < 0.001$; one-way ANOVA/Bonferroni's multiple comparisons test. **L.** is the quantification of the average number of large mitoGFP puncta per affected cell in the fat body tissues with indicated genotypes. Ri, RNAi*;* OE, overexpression. n = 10; **, $p < 0.01$; ***, $p < 0.001$; one-way ANOVA/Bonferroni's multiple comparisons test. **M, N.** The protein level of Marf was unchanged and the protein level of Drp1 was increased in *Dhpr* RNAi tissues. **N** is the quantification for **M**. n = 3 replicates, 20 individual flies per replicate; N.S., not significant; ***, $p < 0.001$; two-tailed unpaired student t-test. **O**. The alignment of fly Drp1 to human Drp1 showed that cystine^{643} in fly Drp1 is corresponding to cystine^{644} in human Drp1. **P**. The real-time PCR results indicated that the knockdown efficiency of the *Nos* RNAi line was around 40%. Ri, RNAi*;* OE, overexpression. n = 4 replicates, 20 flies per replicate; ***, $p < 0.001$; two-tailed unpaired student t-test.

Figure S10

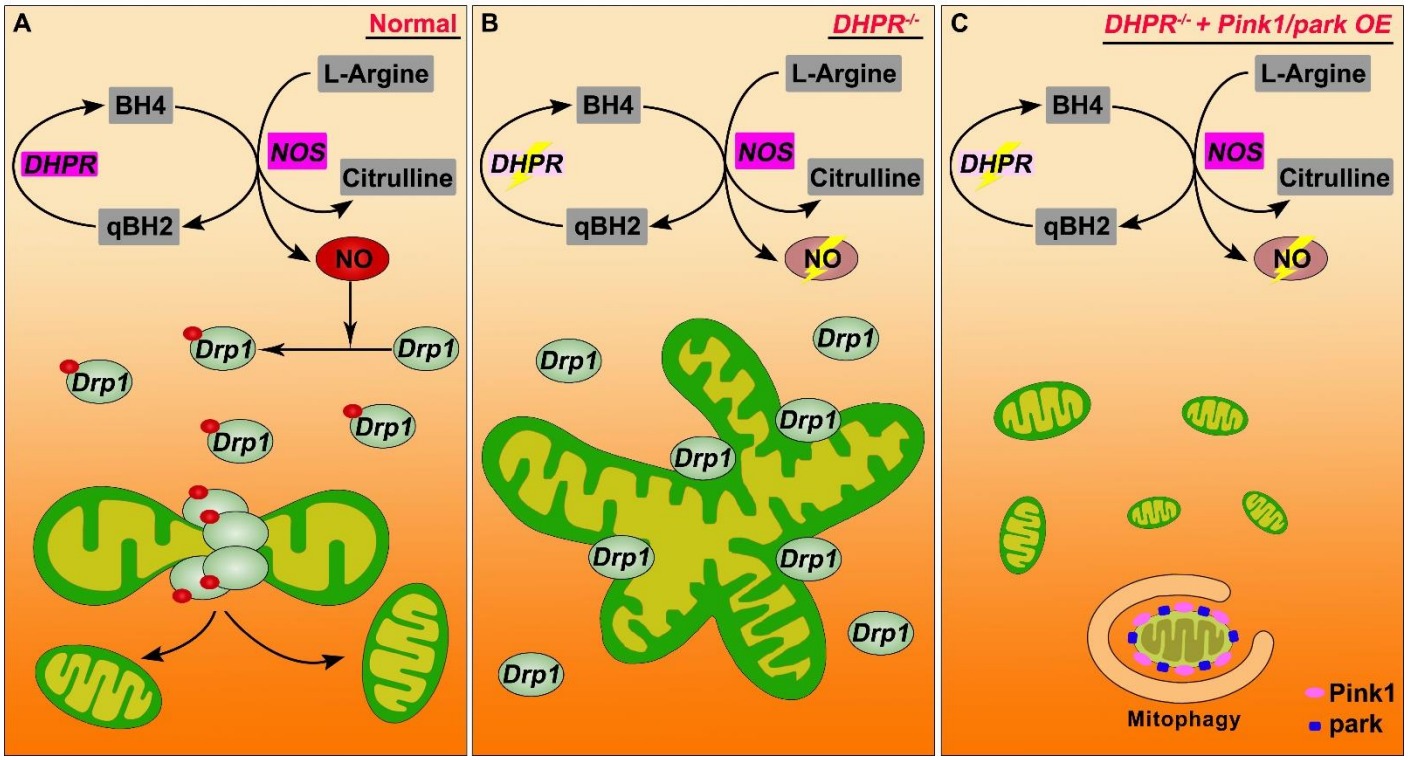

Fig. S10. The model of how Dhpr regulates mitochondrial morphology. A. In wild type tissues, Dhpr regulates BH4 regeneration and participates NO synthesis. NO modifies Drp1 and activates Drp1 activity to maintain normal mitochondrial morphology and tissues homeostasis. **B.** The loss of *Dhpr* reduces NO synthesis. The reduction of sno-Drp1 leads to enlarge of mitochondria and reduction of mitochondrial activity. **C.** The overexpression of *Pink1* or *park* partially rescued mitochondrial defects caused by *Dhpr* RNAi probably through enhanced mitophagy.